Journal of Biomolecular NMR, 10 (1997) 143–164
KLUWER/ESCOM

J-Bio NMR 451

Solution structures of staphylococcal nuclease from multidimensional, multinuclear NMR: Nuclease-H124L and its ternary complex with Ca^{2+} and thymidine-3',5'-bisphosphate*

Jinfeng Wang**, Dagmar M. Truckses, Frits Abildgaard, Željko Džakula, Zsolt Zolnai*** and John L. Markley****

Department of Biochemistry, University of Wisconsin-Madison, 420 Henry Mall, Madison, WI 53706, U.S.A.

Received 8 January 1997
Accepted 28 March 1997

Keywords: Comparison of NMR and X-ray structures; Inhibitor binding; Stereospecific assignments; Distance constraints from NOEs; Torsion angle constraints from J-coupling; Hydrogen bond constraints; Structure refinement

Summary

The solution structures of staphylococcal nuclease (nuclease) H124L and its ternary complex, (nuclease-H124L)•pdTp•Ca^{2+}, were determined by ab initio dynamic simulated annealing using 1925 NOE, 119 ϕ, 20 χ^1 and 112 hydrogen bond constraints for the free protein, and 2003 NOE, 118 ϕ, 20 χ^1 and 114 hydrogen bond constraints for the ternary complex. In both cases, the final structures display only small deviations from idealized covalent geometry. In structured regions, the overall root-mean-square deviations from mean atomic coordinates are 0.46 (±0.05) Å and 0.41 (±0.05) Å for the backbone heavy atoms of nuclease and its ternary complex, respectively. The backbone conformations of residues in the loop formed by Arg^{81}–Gly^{86}, which is adjacent to the active site, are more precisely defined in the ternary complex than in unligated nuclease. Also, the protein side chains that show NOEs and evidence for hydrogen bonds to pdTp (Arg^{35}, Lys^{84}, Tyr^{85}, Arg^{87}, Tyr^{113}, and Tyr^{115}) are better defined in the ternary complex. As has been observed previously in the X-ray structures of nuclease-WT, the binding of pdTp causes the backbone of Tyr^{113} to change from an extended to a left-handed α-helical conformation. The NMR structures reported here were compared with available X-ray structures: nuclease-H124L [Truckses et al. (1996) *Protein Sci.*, **5**, 1907–1916] and the ternary complex of wild-type staphylococcal nuclease [Loll and Lattman (1989) *Proteins Struct. Funct. Genet.*, **5**, 183–201]. Overall, the solution structures of nuclease-H124L are consistent with these crystal structures, but small differences were observed between the structures in the solution and crystal environments. These included differences in the conformations of certain side chains, a reduction in the extent of helix 1 in solution, and many fewer hydrogen bonds involving side chains in solution.

Introduction

Staphylococcal nuclease (nuclease), a 149-residue protein without disulfide bonds, has served for many years as a model system for studies on protein folding, stability, heterogeneity, dynamics as well as protein structure–function relationships. This Ca^{2+}-activated extracellular phosphodiesterase, which degrades both DNA and RNA to 3'-nucleotides, has been isolated from two strains of *Staphylococcus aureus*. By convention, wild-type nuclease (nuclease-WT) has the amino acid sequence of nuclease A from the Foggi strain of *Staphylococcus aureus*, and nuclease-H124L has the sequence of nuclease A from the V8 strain of *S. aureus*. The X-ray crystal structure of the

*Constraint files and atomic coordinates for the 30 conformers that represent the solution structure of unligated nuclease-H124L and those for the 30 conformers that represent the solution structure of the (nuclease-H124L)•Ca^{2+}•-pdTp ternary complex will be deposited with the Protein Databank (PDB, URL http://www.pdb.bnl.gov) as well as with BioMagResBank (BMRB, URL http://www.bmrb.wisc.edu) along with associated NMR parameters under accession numbers 4052 (unligated nuclease) and 4053 (ternary complex).

**Present address: Institute of Biophysics, Academia Sinica, 15 Datun Road, Beijing 100101, China.
***Present address: Mayo Clinic and Mayo Graduate School of Medicine, Rochester, MN 55905, U.S.A.
****To whom correspondence should be addressed.

ternary complex of nuclease-WT with thymidine-3',5'-bisphosphate (pdTp) and Ca^{2+} was determined in the laboratories of Cotton and Hazen (Cotton et al., 1979) and was refined subsequently by Loll and Lattman (1989). Also, refined crystal structures have been reported for unligated nuclease-WT (Hynes and Fox, 1991), unligated nuclease-H124L (Truckses et al., 1996), and several mutant nucleases (Hynes et al., 1989,1994; Stites et al., 1991; Hodel et al., 1993,1995; Keefe et al., 1993; Libson et al., 1994; Truckses et al., 1996).

Although assignments of NMR resonances for nuclease-WT (Torchia et al., 1988,1989), nuclease-H124L (Wang et al., 1990a,b,c,1992a,b), and three mutants (Baldisseri et al., 1991) were obtained, no full solution structure has been reported. Here we describe the refined solution structures of nuclease-H124L and the (nuclease-H124L)•pdTp•Ca^{2+} ternary complex calculated with structural constraints derived from NMR data. They are compared with one another and with the respective X-ray structures. These solution structures provide further information about the structure and dynamics of this protein in solution and improve our understanding of the changes caused by complexation with the inhibitor and calcium.

Materials and Methods

Sample preparation

Protein samples were produced and purified as described in previous studies (Wang et al., 1990a,c; Royer et al., 1993), with stable isotope labeled amino acid precursors added to the growth medium as appropriate. For the preparation of nuclease-H124L labeled uniformly with ^{13}C and ^{15}N (all sites labeled to 98% and 95%, respectively), $(^{15}NH_4)_2SO_4$ and ^{13}C-labeled glucose were substituted in place of the respective unlabeled compounds. Similarly, 'block' ^{13}C-labeled valine and leucine (Tate et al., 1995), obtained as a generous gift from M. Kainosho of Tokyo Metropolitan University, were incorporated into separate samples of nuclease-H124L. The preparation of deuterated samples as well as uniformly ^{15}N-labeled samples has been described previously (Wang et al., 1990a,c). All NMR samples contained 3.5–5.0 mM protein (or complex) and 300 mM KCl; the pH meter reading of samples dissolved in H_2O was 5.1 and that of samples in D_2O was 5.5.

NMR spectroscopy

Table 1 summarizes the acquisition parameters for the NMR experiments used in determining the solution structure of nuclease-H124L and its ternary complex. Results from previously reported (Wang et al., 1990a,c,1992a,b) 2D and 3D homonuclear and heteronuclear experiments were also used and included in the table for completeness. All NMR data were acquired at a temperature of 318 K on Bruker AM500 or AM600 spectrometers. The 3D and 4D triple-resonance data were collected on a Bruker AM500 instrument modified to include triple-resonance capabilities and (for some experiments) single-axis gradient hardware (Mooberry et al., 1994). Unless otherwise stated, solvent suppression was achieved by on-resonance low-power presaturation of the water signal during the relaxation delay, and quadrature detection in the indirectly detected dimensions was obtained with States-TPPI phase cycling (Marion et al., 1989b). Most triple-resonance experiments were collected with initial delays in the indirect dimensions set to give zero- and first-order phase corrections of 90° and −180°, respectively. Spectra were processed on Silicon Graphics workstations using the Felix software package (Biosym Technologies Inc., San Diego, CA, U.S.A.). When appropriate, time domain convolution (Marion et al., 1989a) was used to remove the residual H_2O signal during processing. For the 3D and 4D experiments, the time domain data in the indirectly detected dimensions were extended by 50% using standard linear prediction techniques or by 100% for constant time data using mirror image linear prediction. The processing of the 4D HN(CO)CAHA and HNCAHA data sets was aided by time domain analysis of the indirectly detected dimensions using the CHIFIT software package (Chylla and Markley, 1995). All spectra were referenced to internal TSP (0.0 ppm) in the ^1H dimensions. The ^{13}C and ^{15}N chemical shifts were referenced indirectly to TSP using the ratios 0.251449530 and 0.101329118, respectively, for the zero-point frequencies (Wishart et al., 1995).

Two-dimensional homonuclear E.COSY (Griesinger et al., 1982) experiments at 600 MHz were recorded of uniformly 50% ^2H-labeled nuclease-H124L (in the free state and the ternary complex) in D_2O. Uniformly ^{15}N-labeled nuclease-H124L in H_2O was used to collect 2D ^1H-^{15}N HMQC-J (Forman-Kay et al., 1990; Kay and Bax, 1990) spectra at 600 MHz using time-proportional phase incrementation (TPPI) (Marion and Wüthrich, 1983). The $^3J_{H^NH^\alpha}$ coupling constants were extracted using the program HMQCJFIT (Goodgame and Geer, 1993). Two-dimensional homonuclear DQF-COSY experiments (Rance et al., 1983) were acquired of unlabeled nuclease-H124L in the binary complex with Ca^{2+} and pdTp, respectively, in D_2O. Two-dimensional NOESY experiments (Jeener et

Abbreviations: nuclease, staphylococcal nuclease; nuclease-H124L, recombinant nuclease containing leucine at position 124 (sequence identical to that of nuclease A produced by the V8 strain of *Staphylococcus aureus*); nuclease-WT, recombinant nuclease containing histidine at position 124 (sequence identical to that of nuclease A produced by the Foggi strain of *S. aureus*); pdTp, thymidine-3',5'-bisphosphate; rms, root mean square; rmsd, root-mean-square deviation. The nomenclature for atom names follows the recommendations of the IUPAC-IUB Commission on Biochemical Nomenclature [(1970) *Biochemistry*, **9**, 3471–3479].

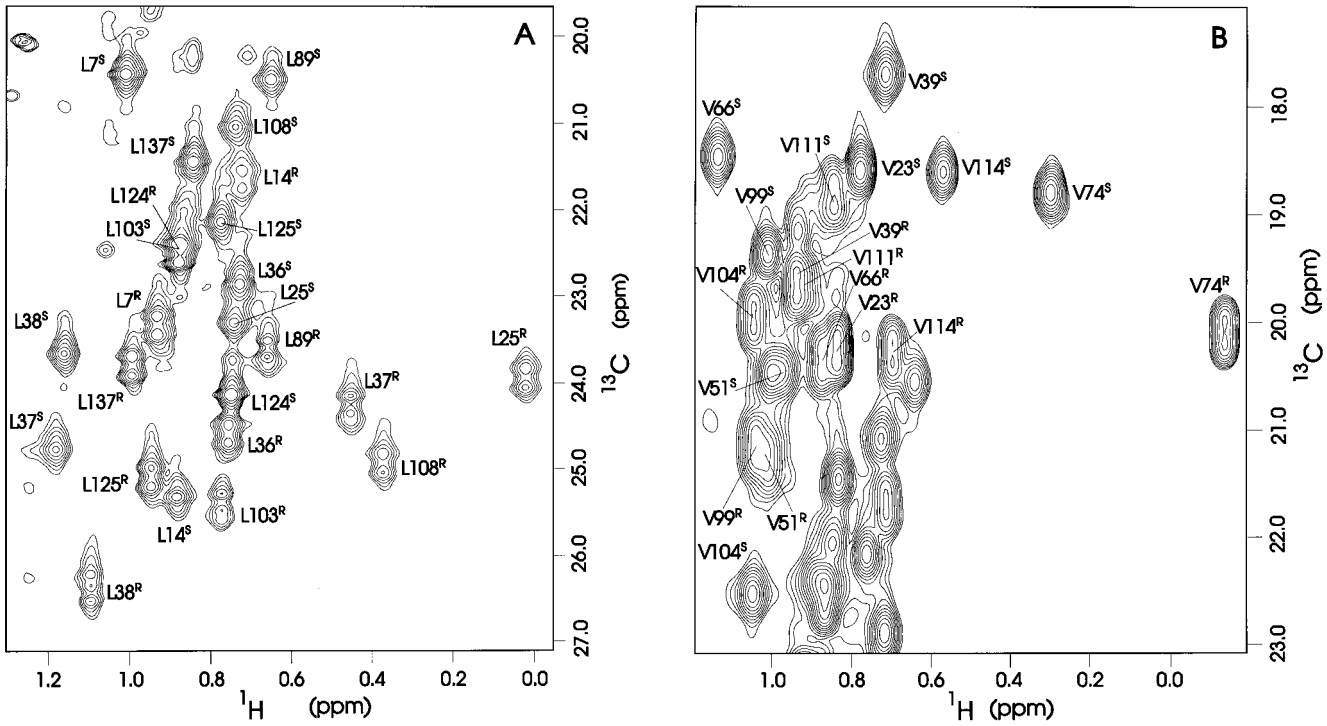

Fig. 1. Methyl region of the 2D ^{1}H-^{13}C HMQC spectrum of staphylococcal nuclease-H124L isolated from *E. coli* grown on media containing (A) block ^{13}C-labeled leucine and (B) block ^{13}C-labeled valine. As described in more detail in the text, ^{1}H-^{13}C cross peaks from *pro-R* methyls are doublets whereas signals from *pro-S* methyls are singlets. Methyl signals are labeled by the one-letter amino acid code and residue number, with superscripts R and S indicating the chiral assignments.

al., 1979) were acquired at 600 MHz with a mixing time of 250 ms using uniformly 50% ^{2}H-labeled nuclease-H124L (in the free state and the ternary complex) in D_2O and H_2O. Three-dimensional ^{1}H-^{15}N NOESY-HMQC (Marion et al., 1989c) spectra were recorded at 600 MHz on a uniformly ^{15}N-labeled nuclease-H124L (in the free state and the ternary complex) in H_2O. A mixing time of 120 ms was used. A 250 ms ^{1}H-^{15}N 3D HMQC-NOESY-HMQC spectrum (Ikura et al., 1990) was acquired at 600 MHz for ^{15}N-labeled nuclease-H124L in the ternary complex. Two-dimensional ^{1}H-^{13}C HMQC data at 600 MHz were acquired of nuclease-H124L (in the free state and the ternary complex) selectively labeled with either the block ^{13}C-labeled valine or leucine (Tate et al., 1995). Phase-sensitive data were collected using TPPI (Marion and Wüthrich, 1983). Three-dimensional HNCO, 3D HNCA (Grzesiek and Bax, 1992), 4D HNCAHA (ternary complex only), and 4D HN(CO)CAHA (Kay et al., 1992) data were collected on samples, dissolved in H_2O, of [U 98% ^{13}C, U 99% ^{15}N]-nuclease-H124L and its ternary complex with pdTp and calcium ion. Three-dimensional HCCH-COSY (Bax et al., 1990) and 3D HCCH-TOCSY (Kay et al., 1993) data were collected on samples, dissolved in D_2O, of [U 98% ^{13}C, U 99% ^{15}N]-nuclease-H124L and its ternary complex. Undesired transverse magnetization in the HCCH-TOCSY experiments was purged by the use of pulsed field gradients (Bax and Pochapsky, 1992); the mixing time (FLOPSY-8 scheme) was 17 ms.

Resonance assignments

The majority of resonances in the spectra of nuclease-H124L and its ternary complex have been assigned previously (Wang et al., 1990a,b,c,1992a,b). These assignments, especially those of side chains, were extended with the help of triple-resonance and ^{1}H-^{13}C heteronuclear experiments (Table 1).

Stereospecific assignments

Stereospecific ^{1}H and ^{13}C assignments of the methyl groups of nine valines and 12 leucines were obtained from the 2D ^{1}H-^{13}C HMQC spectra of two protein samples that incorporated, respectively, block ^{13}C-labeled valine or leucine (Fig. 1). The block labeled amino acids were isolated from proteins prepared by microbial fermentation, using a mixture of 98% ^{13}C [$^{13}C_6$]glucose and unlabeled glucose at 15% and 85%, respectively, as the sole carbon source (Tate et al., 1995). The resulting ^{13}C labeling patterns for valine and leucine reflect the mechanism (including the stereospecificity) of the biosynthetic pathway. The majority of the valine molecules that contain ^{13}C at the C^{γ} position are labeled with ^{13}C at the *pro-R* methyl carbon but not the *pro-S* methyl carbon; whereas most of the valine molecules that contain ^{12}C at the C^{γ} position are labeled with ^{13}C at the *pro-S* methyl carbon but not the *pro-R* methyl carbon. Similarly, the majority of the leucine molecules that contain ^{13}C at the C^{δ} position are labeled with ^{13}C at the *pro-R* methyl carbon but not the

TABLE 1
PARAMETERS FOR NMR EXPERIMENTS[a]

Experiment	Parameters[b]					
	Dimension	Nucleus	Time points	Frequency points	Acquisition time (ms)	Carrier frequency (ppm)
2D NOESY[c,d,e,f]	t_1	^1H	750[g]	4096	53.3	4.53
	t_2	^1H	4096[g]	4096	29.1	4.53
2D NOESY[c,d,e,h]	t_1	^1H	698[g]	4096	46.9	4.53
	t_2	^1H	4096[g]	4096	274	4.53
3D NOESY- HMQC[d,e,i,j]	t_1	^1H	256[g]	256	17.7	4.53
	t_2	^{15}N	28	64	12.3	119.4
	t_3	^1H	512[g]	512	70.7	7.55
3D HMQC-NOESY-HMQC[d,e,j]	t_1	^{15}N	32	64	14.1	119.4
	t_2	^{15}N	64	128	28.2	119.4
	t_3	^1H	2048[g]	2048	141.3	4.53
2D E.COSY[c,k]	t_1	^1H	600[g]	4096	46.2	4.53
	t_2	^1H	4096[g]	4096	315	4.53
2D E.COSY[c,l]	t_1	^1H	800[g]	4096	61.6	4.53
	t_2	^1H	4096[g]	4096	315	4.53
2D HMQC-J[d,e,j]	t_1	^{15}N	878[g]	4096	200	119.9
	t_2	^1H	4096[g]	4096	274	4.53
2D HMQC-J[d,e,i]	t_1	^{15}N	917[g]	4096	209	119.9
	t_2	^1H	4096[g]	4096	274	4.53
2D DQF-COSY[c,k,l,m]	t_1	^1H	51[g]	4096	39.4	4.53
	t_2	^1H	4096[g]	4096	315	4.53
2D DQF-COSY[c,n]	t_1	^1H	600[g]	4096	46.2	4.53
	t_2	^1H	4096[g]	4096	315	4.53
2D HMQC[d,o]	t_1	^{13}C	480[g]	2048	94.6	21.4
	t_2	^1H	2048[g]	2048	157.5	4.53
2D HMQC[d,p]	t_1	^{13}C	410[g]	2048	80.8	21.4
	t_2	^1H	2048[g]	2048	157.5	4.53
2D HMQC[d,q,r]	t_1	^{13}C	512[g]	2048	31.7	38.8
	t_2	^1H	2048[g]	2048	157.5	4.53
3D HNCO[d,s]	t_1	^{15}N	48	256	23.3	117.9
	t_2	^{13}C	64	256	35.8	175.0
	t_3	^1H	1024	2048	158	4.53
3D HNCO[d,t]	t_1	^{15}N	55	256	26.7	117.9
	t_2	^{13}C	64	256	35.8	175.0
	t_3	^1H	1024	2048	158	4.53
3D HNCA[d,s]	t_1	^{15}N	36	256	17.5	117.9
	t_2	^{13}C	64	256	11.5	59.2
	t_3	^1H	1024	2048	158	4.53
3D HNCA[d,t]	t_1	^{15}N	32	256	15.6	117.9
	t_2	^{13}C	64	256	11.5	59.2
	t_3	^1H	1024	2048	158	4.53
4D HNCAHA[d,t]	t_1	^{13}C	10	64	3.62	53.4
	t_2	^1H	8	64	3.55	4.53
	t_3	^{15}N	16	64	7.78	117.9
	t_4	^1H	512	1024	78.8	4.53
4D HN(CO)CAHA[d,s,t]	t_1	^{13}C	9	64	3.26	53.4
	t_2	^1H	8	64	3.55	4.53
	t_3	^{15}N	16	64	7.78	117.9
	t_4	^1H	512	1024	78.8	4.53
3D HCCH-COSY[c,s,t]	t_1	^1H	128	256	32.0	2.85
	t_2	^{13}C	32	128	8.32	42.5
	t_3	^1H	1024	2048	158	2.85

TABLE 1
(continued)

Experiment	Parameters[b]					
	Dimension	Nucleus	Time points	Frequency points	Acquisition time (ms)	Carrier frequency (ppm)
3D HCCH-TOCSY[c,s,t]	t_1	^1H	128	256	28.2	3.07
	t_2	^{13}C	128	256	14.6	42.5
	t_3	^1H	512	1024	112.6	3.07

[a] Data were collected at 500.13 MHz for ^1H unless otherwise stated.
[b] Number of points given in the time domain refers to complex points unless otherwise stated. Number of points in the frequency domain of processed data refers to real points.
[c] In D_2O.
[d] In H_2O.
[e] Data were collected at 600.13 MHz for ^1H.
[f] Nuclease-H124L 50% uniformly labeled with ^2H.
[g] Real points.
[h] Nuclease-H124L 50% uniformly labeled with ^2H in the ternary complex.
[i] Uniformly ^{15}N-labeled nuclease-H124L.
[j] Uniformly ^{15}N-labeled nuclease-H124L in the ternary complex.
[k] Nuclease-H124L at natural isotopic abundance.
[l] Nuclease-H124L at natural isotopic abundance in the ternary complex.
[m] Nuclease-H124L at natural isotopic abundance in the binary complex with Ca^{2+}.
[n] Nuclease-H124L at natural isotopic abundance in the binary complex with pdTp.
[o] Nuclease-H124L selectively labeled with [$^{13}C^{\beta,\gamma l}$]-Val.
[p] Nuclease-H124L selectively labeled with [$^{13}C^{\gamma,\delta 1}$]-Leu.
[q] Nuclease-H124L selectively labeled with [$^{13}C^{\beta,\gamma l}$]-Val in the ternary complex.
[r] Nuclease-H124L selectively labeled with [$^{13}C^{\gamma,\delta 1}$]-Leu in the ternary complex.
[s] Uniformly ^{13}C,^{15}N-labeled nuclease-H124L.
[t] Uniformly ^{13}C,^{15}N-labeled nuclease-H124L in the ternary complex.

pro-S methyl carbon; whereas most of the leucine molecules that contain ^{12}C at the C^{δ} position are labeled with ^{13}C at the *pro-S* methyl carbon but not the *pro-R* methyl carbon. Thus, for both valine and leucine, the ^{13}C resonance of each *pro-R* methyl group is predominantly a doublet as the result of one-bond ^{13}C-^{13}C coupling, whereas the resonance for each *pro-S* methyl group is chiefly a singlet (Fig. 1).

An initial set of stereospecific assignments for resonances from non-degenerate (non-overlapped) β-methylene protons was obtained by the analysis of $^3J_{H^{\alpha}H^{\beta}}$ coupling constants and intraresidue NOE intensities (Zuiderweg et al., 1985; Hyberts et al., 1987; Arseniev et al., 1988). This approach yielded stereospecific assignments for 21 residues of unligated and 25 residues of ligated nuclease-H124L. Furthermore, diastereotopic, non-degenerate β-protons and, in some cases, degenerate β-protons were assigned by the following procedure. For diastereotopic non-degenerate β-protons, a tentative assignment of the two β-protons was made. If the calculated set of structures revealed a well-defined conformation for the given side chain, and the distances from these β-protons to the surrounding structure were consistent with the experimental data, the assumed chirality was employed in successive structure calculations. Otherwise, the tentative assignments were interchanged, and the analysis was repeated. This approach led to stereospecific assignments for 54 and 49 resolved pairs of β-proton resonances in nuclease-H124L and its ternary complex, respectively. The additional non-degenerate β-proton resonances assigned stereospecifically for unligated nuclease but not for the ternary complex were those of Gln^{30}, His^{46}, Lys^{78}, Lys^{84}, and Arg^{87}. The distance constraints to degenerate β-methylene protons were attributed to one proton stereospecifically if the set of structures demonstrated that the local conformation was well-defined and if only one of the β-protons was close to the NOE partners. Similar adjustments were made for degenerate $^1H^{\delta}$ and $^1H^{\varepsilon}$ signals from aromatic rings.

TABLE 2
SUMMARY OF EXPERIMENTAL CONSTRAINTS USED FOR THE STRUCTURE CALCULATIONS[a]

Constraints	Nuclease-H124L	Nuclease-H124L ternary complex
NOE distance		
Intraresidue	764	762
Sequential: $(i-j)=1$	494	530
Medium-range: $1<(i-j)<5$	248	258
Long-range: $(i-j)\geq 5$	419	440
Intramolecular (pdTp)[b]		27
Intermolecular (pdTp–nuclease)		13
Hydrogen bonds		
Nuclease	112	114
Intermolecular (pdTp–nuclease)		6
Torsion angles		
φ torsion angles	119	118
χ^1 torsion angles	20	20
pdTp ribose torsion angles[b]		45
Stereospecific assignment		
β-protons	54	49
γ-methyl groups of valine	9	9
δ-methyl groups of leucine	12	12

[a] Experimental constraints were imposed on residues Lys^7–Asp^{143}.
[b] These constraints were derived from the conformation of pdTp in the crystal structure of the nuclease-WT ternary complex (Loll and Lattman, 1989).

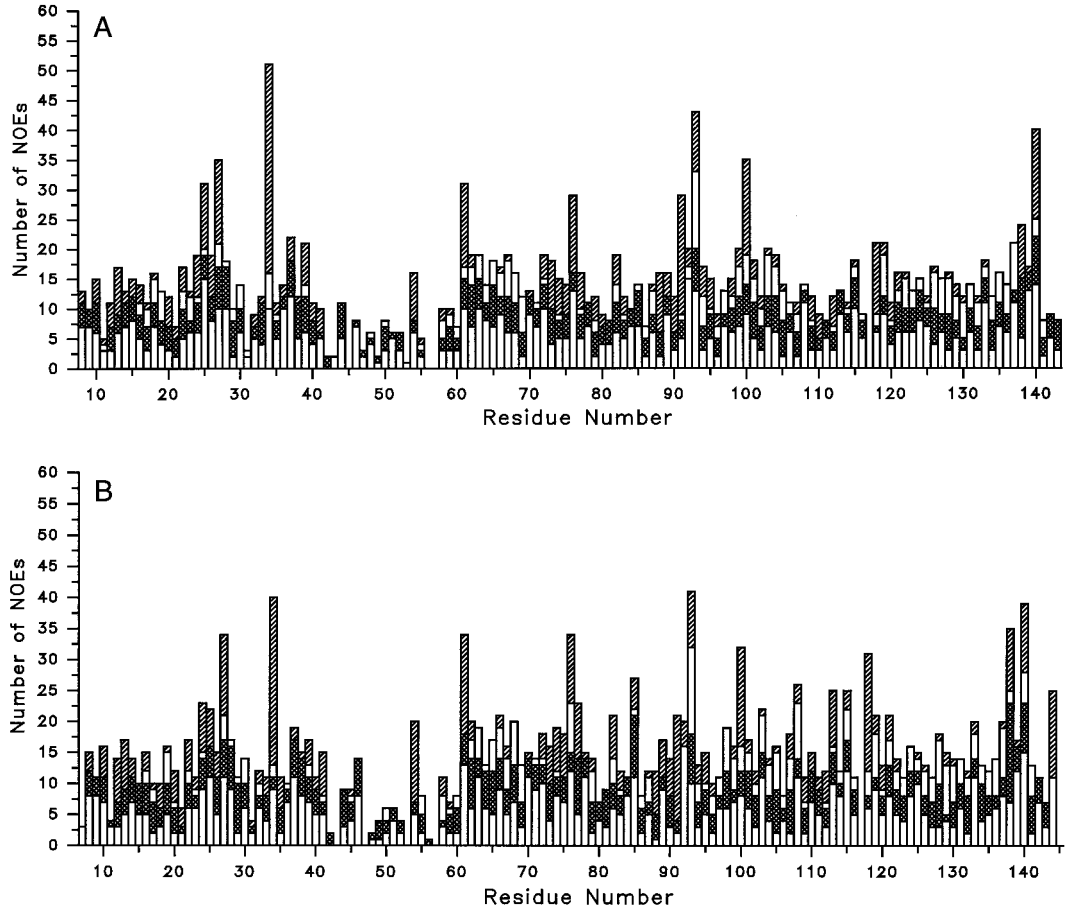

Fig. 2. Plot of the number of NOE distance constraints for every residue: (A) nuclease-H124L; (B) (nuclease-H124L)•pdTp•Ca^{2+} ternary complex; pdTp is shown as residue 144. The constraints are specified as follows: white (lower) – intraresidue; crosshatch – sequential NOE constraints ((i – j) = 1); white (upper) – medium-range NOEs ((i – j) = 2–4); diagonal crosshatch (top) – long-range NOEs including intermolecular protein–pdTp NOEs in the case of the ternary complex.

NOE distance constraints

Interproton distance constraints used for the structure calculations are summarized in Table 2 and Fig. 2. They were derived from NOE cross-peak intensities, which were determined by measuring cross-peak volumes and counting cross-peak contour levels in the 2D ^{1}H NOESY and 3D ^{1}H-^{15}N NOESY-HMQC spectra (Wang et al., 1990c, 1992a,b) previously recorded on samples of 50% deuterated and 95% uniformly ^{15}N-labeled protein, respectively. The mixing times were 250 and 125 ms for the 2D and 3D experiments, respectively. All the constraints were combined to make one set of distance constraints for nuclease-H124L and one for the nuclease-H124L ternary complex.

For calibration purposes, the NOEs were divided into four types: NOEs between pairs of single non-amide protons, NOEs between a single (non-amide) proton and a methyl group, NOEs between pairs of methyl groups, and NOEs involving amide protons. The intensities and contour levels measured for the different types of NOE cross peaks were converted to distances by calibration against NOEs between pairs of protons at known fixed distances (Momany et al., 1975) or against NOEs corresponding to estimated distances in the case of NOEs to amide protons. The $H^{\varepsilon 3}$–$H^{\zeta 3}$ distance of Trp^{140} (2.5 Å) and the distance between the centroids of the two γ-methyl groups of Val^{74} (3.2 Å) were used as calibration distances for NOEs between single protons and for NOEs between methyl groups, respectively. The distance between the α-proton and the centroid of the methyl β-protons of Ala^{130} (3.0 Å) was used to calibrate NOEs between a single proton and a methyl group. Ala^{130} was chosen (among nine alanines) because the intraresidue ^{1}H NOE cross peaks of Ala^{130} are isolated from others in all proton–proton connectivity regions. Also the amide proton of Ala^{130} exchanges slowly with bulk water. Thus, the H^{N}–H^{α} (2.9 Å) and H^{N}–H^{β} (2.6 Å) distances of Ala^{130} were used for the calibration of NOEs to amide protons in the 3D ^{1}H-^{15}N spectra; these two distances were estimated from 2D ^{1}H NOESY (H_2O) spectra by reference to other cross peaks corresponding to known fixed distances. The rigid model approximation was used in converting NOE intensities to interproton distances (Gondol and Van Binst, 1986), and distance constraints involving pseudoatoms were taken into consideration as described by Wüthrich

et al. (1983). This led to four upper-bound distance constraints: 2.7, 3.5, 5.3, and 6.5 Å. The 6.5 Å upper bound was set somewhat arbitrarily after inspection of the whole data set and considering the possible effects of spin diffusion. A lower bound of 1.8 Å was used for all four ranges.

Hydrogen bond constraints

The presence of backbone hydrogen bonds in regions of regular secondary structure was deduced from a qualitative interpretation of NOE patterns according to criteria laid out by Wagner et al. (1987) and from experimental amide hydrogen exchange rates (Wang et al., 1990c; Loh et al., 1993). Forty-eight hydrogen bonds were found in both nuclease-H124L and its ternary complex. In calculations of both structures, each of these hydrogen bonds was represented by two distance constraints: 1.8–2.3 Å for the distance between the hydrogen and the acceptor atom and 2.4–3.3 Å for the distance between the donor heavy atom and the acceptor atom. Additional hydrogen bonds within and between loop and turn regions were determined by the following strategy. Ten structures were calculated on the basis of all initial experimental constraints including hydrogen bonding constraints for regular secondary structure. These structural models were inspected for the presence of additional hydrogen bonds. A hydrogen bond was assumed to be present if the distance between the acceptor and donor heavy atoms was less than 3.4 Å and if the donor atom···hydrogen···acceptor atom angle was greater than 110°. This analysis suggested the following additional hydrogen bonds in both structures: Arg^{35} H^N···Gly^{88} O, Gly^{88} H^N···Thr^{33} O, Asp^{83} H^N···Arg^{87} O, Leu^{89} H^N···Arg^{81} O, Ile^{18} H^N···Thr^{22} O, and Asp^{19} H^N···Thr^{22} O. The analysis also indicated additional hydrogen bonds in unligated nuclease for Leu^{36} H^N···Asp^{21} O and Leu^{37} H^N···Ala^{90} O and in the ternary complex for Gly^{86} H^N···Asp^{83} O, Gly^{79} H^N···Asn^{118} $O^{\delta 1}$, and Glu^{122} H^N···Asn^{119} O. Table 1 of the Supplementary Material lists the geometry of these hydrogen bonds in the 10 preliminary structural models, and is available upon request. The existence of most of these additional hydrogen bonds is supported by slow hydrogen exchange rates (Wang et al., 1990c; Loh et al., 1993). Thus, in the final structure calculations these hydrogen bonds were included as constraints. They appear to stabilize the conformation of loop and turn regions, leading to reduced rmsd values.

Torsion angle constraints

Backbone ϕ torsion angle constraints were obtained for 119 and 118 residues of nuclease-H124L and its ternary complex (Table 2), respectively, from vicinal spin–spin coupling constants, $^3J_{H^NH^\alpha}$ (Pardi et al., 1984). For $^3J_{H^NH^\alpha} < 6.0$ Hz, ϕ was restrained near −60°; for $^3J_{H^NH^\alpha} > 9.0$ Hz, ϕ was restrained between −100° and −140°; and for $^3J_{H^NH^\alpha}$ values between 6.0 and 9.0 Hz, ϕ was restrained between −80° and −160°. For residues with 6.0 Hz $< {}^3J_{H^NH^\alpha} <$ 7.0 Hz and with a strong H^N–H^α intraresidue NOE, ϕ was restrained between +50° and +80° (Wüthrich, 1986; Kline et al., 1988). Errors of ±50° and ±30° were allowed, respectively, for ϕ constraints in nuclease-H124L and its ternary complex. For each structure, 20 χ^1 torsion angle constraints were obtained from $^3J_{H^\alpha H^\beta}$ coupling constants measured as passive couplings in E.COSY spectra (Griesinger et al., 1982). An error range of ±30° and ±20°, respectively, was used for χ^1 angle constraints in nuclease-H124L and its ternary complex. Forty-five torsion angle constraints for ribose protons of pdTp, obtained from the X-ray structure of the nuclease-WT ternary complex (Loll and Lattman, 1989), were used to restrain the conformation of pdTp.

All peptide bonds were restrained to be planar and *trans*, with the exception of that between Lys^{116} and Pro^{117}, which was constrained to be planar and *cis* (Hinck et al., 1993). One-dimensional ^{1}H NMR spectra have shown that approximately 10% of the molecules have a *trans* Lys^{116}–Pro^{117} peptide bond. However, it has not been possible to make extensive separate assignments for this minor population.

Constraints for pdTp

The nucleotide inhibitor pdTp was modeled in the structures of the complex either as a flexible molecule restrained by 11 intramolecular NOEs, 13 intermolecular protein–pdTp NOEs and six intermolecular hydrogen bond constraints, or as a rigid structure fixed by 72 (distance and torsion angle) constraints derived from its conformation in the X-ray structure of the nuclease-WT ternary complex (Loll and Lattman, 1989) and the 13 protein–pdTp NOE constraints. With the flexible model, the position and conformation of pdTp in the complex were undetermined. The final family of structures reported here are ones in which the pdTp conformation was fixed. This had no effect on the conformation of the protein but made it easier to visualize the position of the nucleotide.

A preliminary set of structures for the nuclease-H124L ternary complex was derived without hydrogen bonds to pdTp. Of these structures, 50% or more showed average distances of 4.4 Å between the Tyr^{85} O^η and the O3 phosphate oxygen of pdTp, 3.9 Å between the O5 phosphate oxygen of pdTp and the Arg^{87} $N^{\eta 1}$, and 3.2 Å between the O5 phosphate oxygen of pdTp and the Arg^{35} N^ε. Since this indicated general agreement with the X-ray structure of the (nuclease-WT)•pdTp•Ca^{2+} ternary complex (Loll and Lattman, 1989), the hydrogen bonds between the side-chain donor groups of residues Arg^{35}, Lys^{84}, Tyr^{85}, and Arg^{87}, and the phosphate oxygen acceptor groups of pdTp deduced from the crystal structure were assumed to be present, and constraints at these positions were used in the final structure determinations.

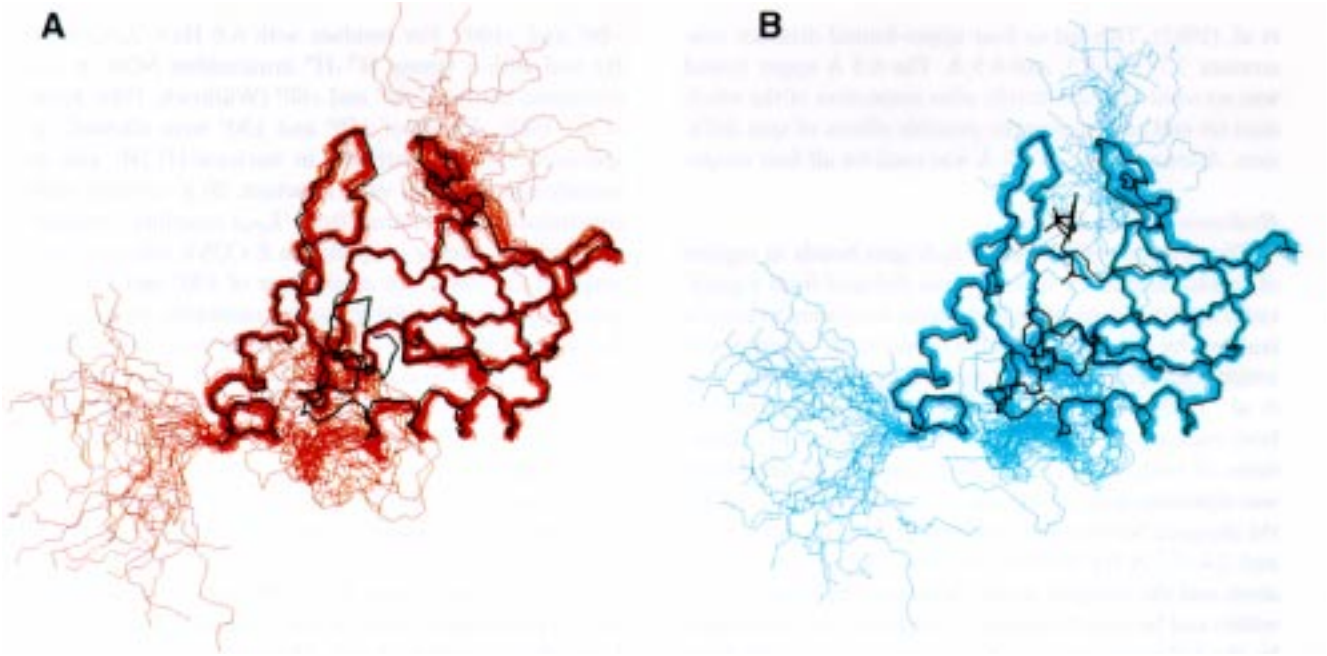

Fig. 3. Superposition of the 30 conformers that represent the NMR-derived solution structure on the corresponding structure determined by X-ray crystal diffraction: (A) solution structure (colored) of nuclease-H124L (this work) and the crystal structure (black) of the same protein (Truckses et al., 1996); (B) solution structure (colored) of the (nuclease-H124L)•pdTp•Ca^{2+} ternary complex (this work) and the crystal structure (black) of the (nuclease-WT)•pdTp•Ca^{2+} ternary complex (Loll and Lattman, 1989).

Strategies used in the structure calculations

The program X-PLOR v. 3.1 (Brünger, 1992) was used for the calculations of 3D structures of nuclease-H124L by ab initio simulated annealing starting from template coordinate sets (Nilges et al., 1991). Extended strands of nuclease-H124L alone and nuclease-H124L with the mononucleotide bisphosphate inhibitor (pdTp) served as the starting templates, respectively, for the structures of nuclease-H124L and the (nuclease-H124L)•pdTp•Ca^{2+} ternary complex. In the ternary complex, the protein chain was designated as segment A and pdTp as segment B. The topology and parameter files used for pdTp were generated by modifying the topology and parameter files for DNA provided with the X-PLOR software package.

TABLE 3
STRUCTURAL STATISTICS

	Nuclease-H124L			Nuclease-H124L ternary complex		
	⟨SA⟩	$\langle SA \rangle_r$	X-ray[a]	⟨SA⟩	$\langle SA \rangle_r$	X-ray[b]
Rmsd from experimental NOE distance constraints (Å)	0.0051 ± 0.0006	0.005	0.082	0.0052 ± 0.0006	0.0045	0.068
Rmsd from experimental torsion angle constraints (°)	0.04 ± 0.02	0.049	0.437	0.08 ± 0.02	0.071	0.584
Rmsd from idealized covalent geometry						
Bonds (Å)	0.0009 ± 0.0001	0.0008	0.009	0.0011 ± 0.0005	0.0009	0.017
Angles (°)	0.23 ± 0.01	0.23	1.693	0.25 ± 0.02	0.25	0.037
Improper (°)	0.20 ± 0.01	0.20	1.225	0.24 ± 0.01	0.24	0.050
X-PLOR energies (kcal mol^{-1})						
E (bond)	2.0 ± 0.2	1.50	459	2.5 ± 0.3	2.14	620
E (angle)	36 ± 1	35.96	2164	42 ± 1	41.4	4078
E (VDW)	1.5 ± 0.7	1.17	234	3 ± 1	1.52	746
E (NOE)	2.7 ± 0.6	2.57	679	2.9 ± 0.7	2.17	478
E (CDIH)	0.02 ± 0.01	0.021	1.69	0.06 ± 0.03	0.056	2.85
E (improper)	7.4 ± 0.4	7.73	12 508	10.4 ± 0.3	10.44	12 371

⟨SA⟩: ensemble of 30 structures; $\langle SA \rangle_{av}$: mean structure obtained by superposition of backbone N, C^{α}, and C atoms for all residues; $\langle SA \rangle_r$: regularized mean structure obtained by restrained regularization of the mean structure (Nilges et al., 1988).

[a] X-ray coordinates are from the 1.7 Å structure of nuclease-H124L (Truckses et al., 1996).

[b] X-ray coordinates are from the 1.65 Å structure of the (nuclease-WT)•pdTp•Ca^{2+} ternary complex (Loll and Lattman, 1989).

The dynamic simulated annealing protocol used was essentially that described in the X-PLOR manual. A soft-square function was used for the distance and torsion angle constraints, and a simple quartic potential was applied for the van der Waals term during the dynamic simulated annealing. Force constants for the NOE-de-

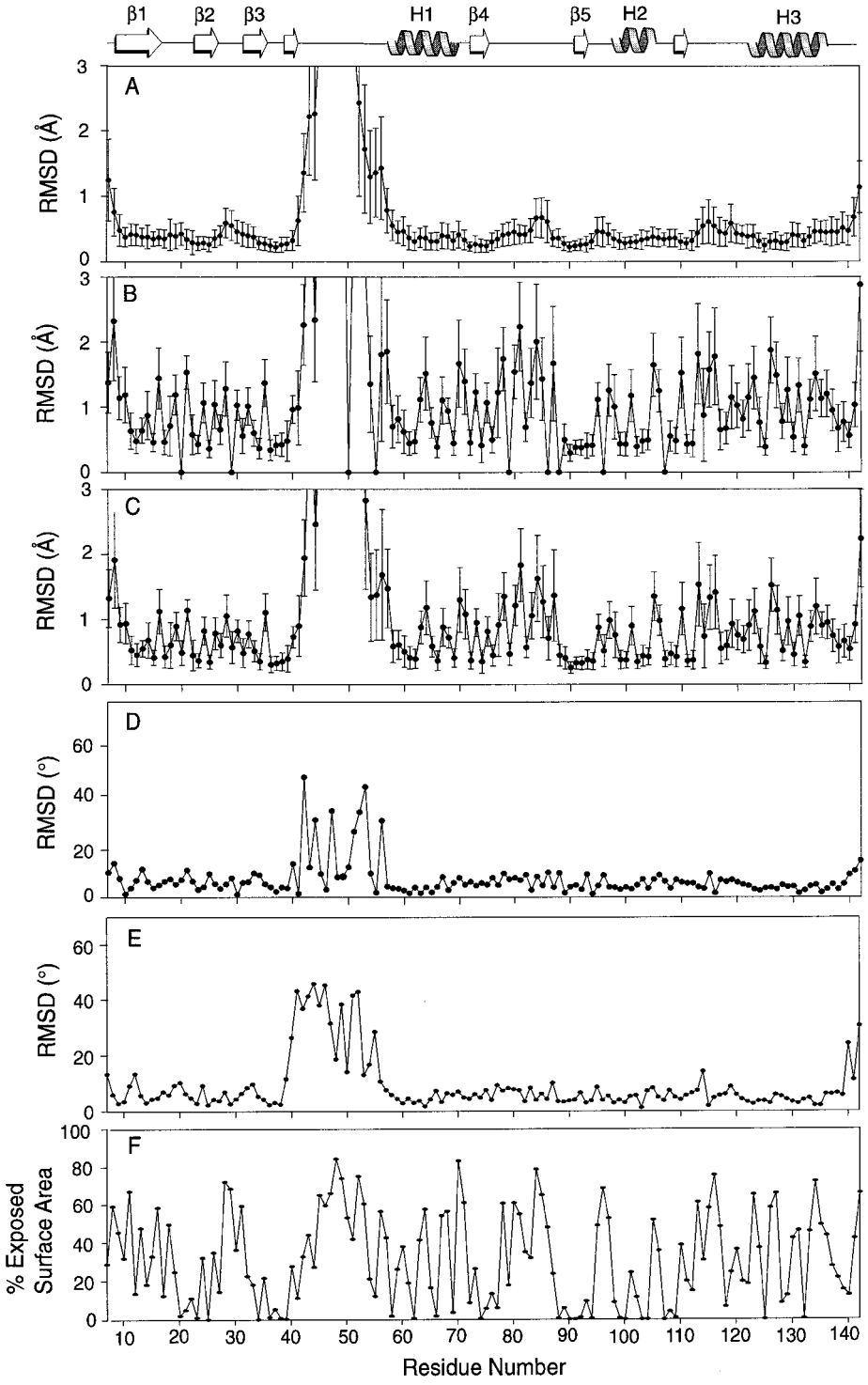

Fig. 4. Plots of various structural parameters versus the residue number of the protein for the 30 conformers that represent the structure of nuclease-H124L. Average rmsd values from the mean structure coordinates (the unstructured ends of the protein (Ala^{1}–Lys^{6} and Asp^{143}–Gln^{149}) are not shown) for (A) backbone heavy atoms (C^{α}, C', N, O), (B) side-chain heavy atoms, and (C) all non-hydrogen atoms. Mean pairwise rmsd values of (D) ϕ and (E) ψ angles among the 30 structures. (F) Average percent solvent accessibility. Solvent-accessible surfaces were calculated using the algorithm of Lee and Richards (1971), as implemented by the program X-PLOR, using a 1.4 Å solvent molecule radius. Fractional solvent accessibility was calculated with respect to Gly-X-Gly tripeptides (Chothia, 1975).

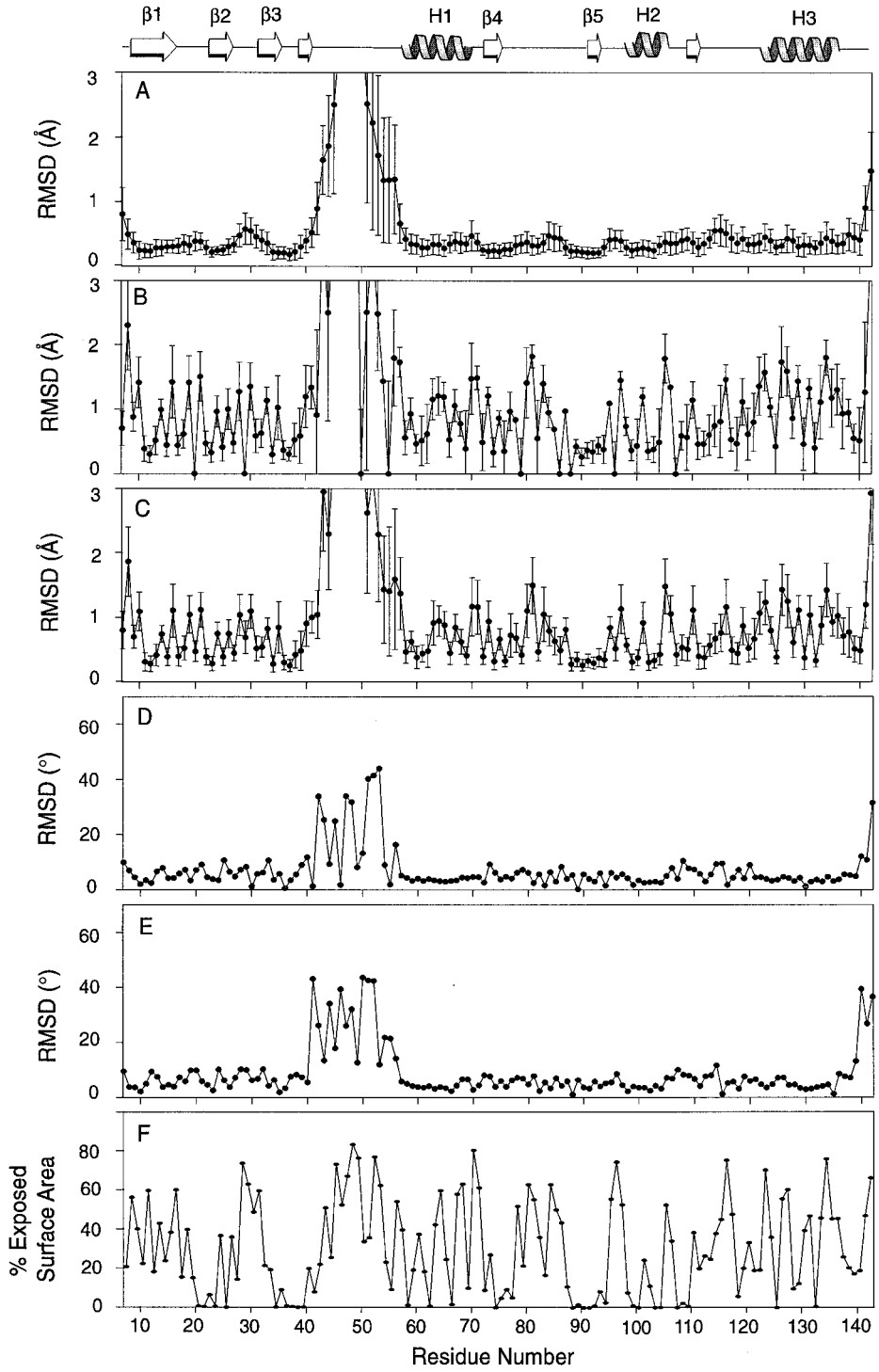

Fig. 5. Plots of various structural parameters versus the residue number of the protein for the 30 conformers that represent the structure of the (nuclease-H124L)•pdTp•Ca^{2+} ternary complex. Average rmsd values from the mean structure coordinates for (A) backbone heavy atoms (C^{α}, C', N, O), (B) side-chain heavy atoms, and (C) all non-hydrogen atoms. Mean pairwise rmsd values of (D) ϕ and (E) ψ angles among the same 30 structures. (F) Average percent surface accessibility calculated as described for Fig. 4.

rived distance constraints were maintained at 50 kcal mol^{-1} $Å^{-2}$ throughout the refinement process. Torsion angle constraints were initialized to 5 kcal mol^{-1} rad^{-2} and increased to 200 kcal mol^{-1} rad^{-2} at the beginning of annealing. The dynamic annealing was carried out over 120 ps of restrained dynamics at high temperature (2000 K). Then, the annealing proceeded stepwise from 2000 to 100 K in 50° decrements, with each step consisting of 1.57 ps of restrained molecular dynamics. The force constant on the repulsive term was increased stepwise during this pro-

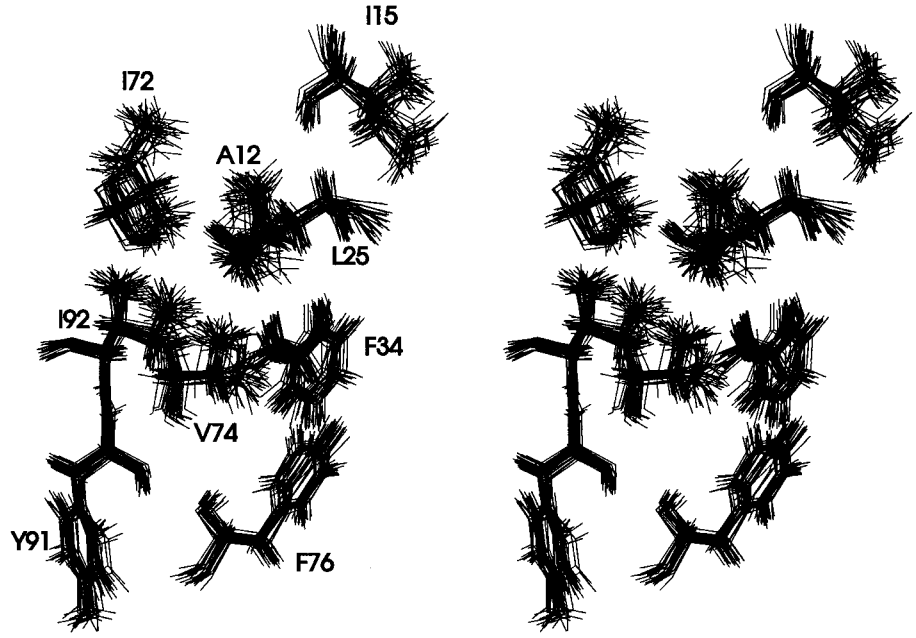

Fig. 6. Stereoview showing the relative positions of the well-defined side chains of residues Ala[12], Leu[25], Ile[72], Val[74], Phe[34], Phe[76], Ile[15], Tyr[91], and Ile[92] in the family of 30 structures of the (nuclease-H124L)•pdTp•Ca^{2+} ternary complex.

cess from 0.003 to 4.0 kcal mol^{-1} $Å^{-4}$. The final structures were the result of 200 subsequent cycles of potential energy minimization. Separate sets of 90 structures were generated for nuclease-H124L and its ternary complex. Structures that showed local structural deviations from the mean coordinates or displayed a large number of violations or higher values for various terms in the target function were excluded from further refinement. All of

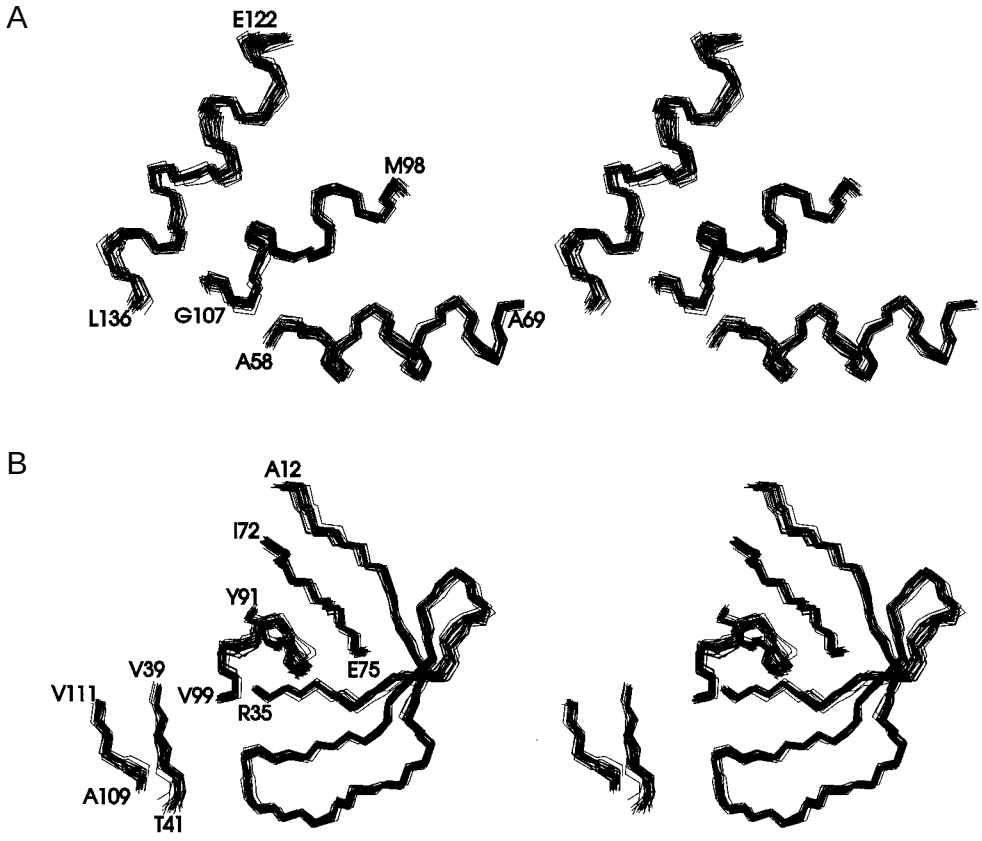

Fig. 7. Stereoscopic views of the secondary structural elements of the (nuclease-H124L)•pdTp•Ca^{2+} ternary complex: (A) α-helix; (B) β-sheet.

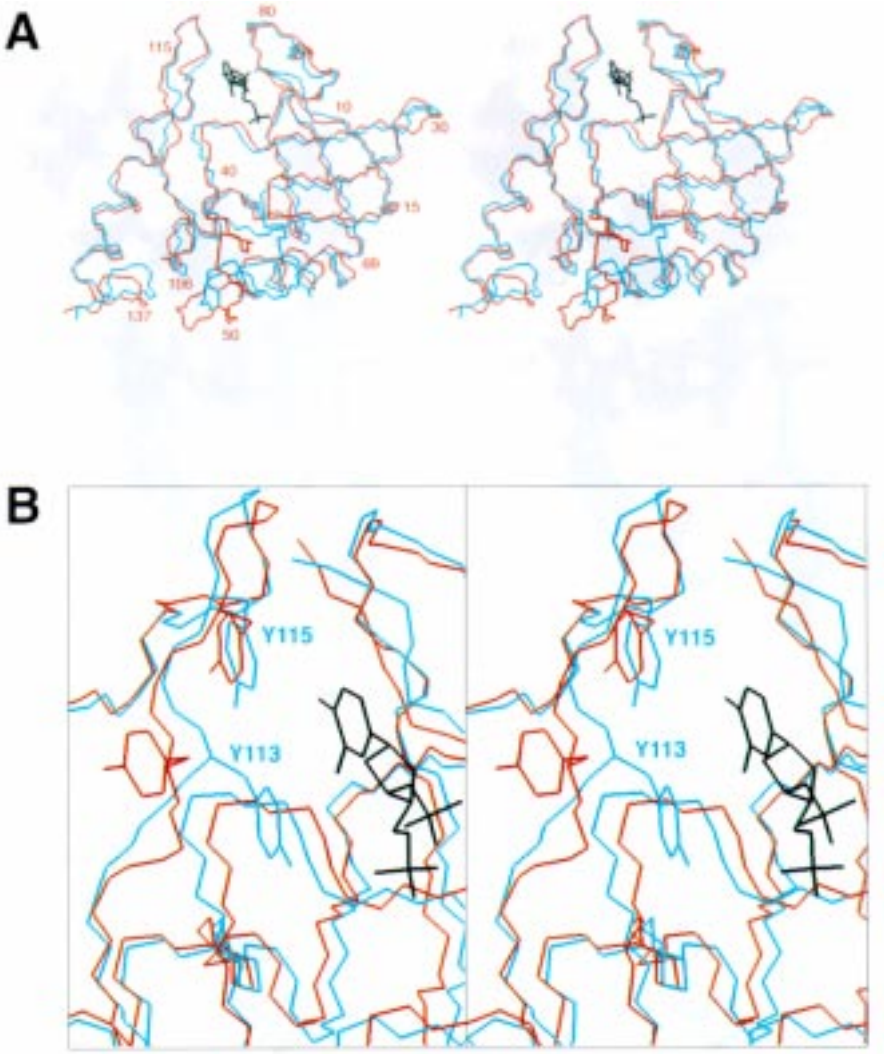

Fig. 8. Superposition of the regularized mean backbone coordinates of the NMR solution structures of nuclease-H124L (red) and the (nuclease-H124L)•pdTp•Ca^{2+} ternary complex (blue). The mean coordinates of the inhibitor, pdTp, are shown in black. (A) View of the whole protein. (B) Close-up of Tyr^{113} whose backbone conformation is different in the two structures. As the result of a conformational change, an NOE builds up between $^1H^{\varepsilon}$ of Tyr^{115} and $^1H^{\delta}$ of Tyr^{113} in the ternary complex but not in unligated nuclease. The positions of the side chains of Tyr^{113} and Tyr^{115} are shown to illustrate this difference between the structures.

the well-refined structures satisfied the experimental constraints. Refined structures that showed relatively high rmsd values with respect to the experimental and geometric constraints were excluded, and a final set of 30 structures was considered for structural analysis. All calculations were carried out on Silicon Graphics computer workstations (4D/220 GTX). The software packages INSIGHTII (v. 2.3, Biosym Technologies), X-PLOR, and HBPLUS (McDonald and Thornton, 1994) were used for structural analysis.

Results and Discussion

Structure calculations

A total of 2176 and 2261 distance, hydrogen bond and torsion angle constraints were used to calculate the structures of nuclease-H124L and the (nuclease-H124L)•pdTp•Ca^{2+} ternary complex, respectively. In each case, the final 30 structures did not violate any NMR distance constraints by more than 0.2 Å, and experimental torsion angle constraints were satisfied to within 5°. Structural statistics for both structures are listed in Table 3.

Backbone conformation

Best-fit superpositions of the backbone heavy-atom coordinates of the 30 structures for nuclease-H124L and its ternary complex, respectively, are shown in Figs. 3A and B. The secondary and tertiary structures are the same as described previously for the crystal structures of nuclease-WT (Loll and Lattman, 1989; Hynes and Fox, 1991) and nuclease-H124L (Truckses et al., 1996); the protein consists of a highly twisted five-stranded β-barrel

TABLE 4
ATOMIC RMS DEVIATIONS

	Nuclease-H124L		Nuclease-H124L ternary complex	
	Backbone atoms[a]	All non-hydrogen atoms	Backbone atoms[a]	All non-hydrogen atoms
Structured regions (His[8]–Thr[41] and Ala[58]–Trp[140])[b]				
$\langle SA \rangle$ against $\langle SA \rangle_{av}$	0.46 ± 0.05	0.91 ± 0.07	0.41 ± 0.05	0.83 ± 0.05
$\langle SA \rangle$ against $(SA)_r$	0.64 ± 0.07	1.30 ± 0.08	0.66 ± 0.06	1.17 ± 0.06
$\langle SA \rangle_{av}$ against $(SA)_r$	0.45	0.92	0.52	0.69
$\langle SA \rangle$ against X-ray	0.6 ± 0.2	1.2 ± 0.7	0.6 ± 0.2	1.1 ± 0.6
$\langle SA \rangle_{av}$ against X-ray	0.52		0.47	
$(SA)_r$ against X-ray	0.66		0.71	
Segment (Pro[42]–Glu[57])[c]				
$\langle SA \rangle$ against $\langle SA \rangle_{av}$	2.0 ± 0.4		1.8 ± 0.5	
$\langle SA \rangle$ against $(SA)_r$	2.4 ± 0.5		2.0 ± 0.6	
$\langle SA \rangle_{av}$ against $(SA)_r$	1.65		1.04	
$\langle SA \rangle$ against X-ray	2.8 ± 0.6		3.2 ± 0.8	
$\langle SA \rangle_{av}$ against X-ray	2.28		2.83	
pdTp[d]				
$\langle SA \rangle$ against $\langle SA \rangle_{av}$			0.6 ± 0.1	
$\langle SA \rangle$ against $\langle SA \rangle_r$			0.7 ± 0.4	

$\langle SA \rangle$: ensemble of 30 structures; $\langle SA \rangle_{av}$: mean structure obtained by superposition of backbone N, C^{α}, and C atoms for all residues; $\langle SA \rangle_r$: regularized mean structure obtained by restrained regularization of the mean structure (Nilges et al., 1988).
[a] The N, C^{α}, and C atoms of the backbone.
[b] The coordinates of His[8]–Thr[41] and Ala[58]–Trp[140] were superimposed.
[c] The coordinates of residues Pro[42]–Glu[57] were superimposed.
[d] The pdTp coordinates were superimposed.

(strands are formed by Lys[9]–Ala[17], Thr[22]–Met[26], Pro[31]–Arg[35], Ile[72]–Phe[76], and Ala[90]–Tyr[93]), three α-helices (Glu[57]–Ala[69], Met[98]–Gln[106], and Glu[122]–Glu[135]), 10 β-turns, and several loop regions. Except for the N- and C-termini (residues Ala[1]–Leu[7] and Ser[141]–Gln[149]) and the flexible loop formed by Pro[42]–Glu[57], the structures are well determined by the NMR data, with rmsd values with respect to the average (⟨rmsd⟩) of 0.46 (±0.05) Å and 0.41 (±0.05) Å, respectively, for the backbone heavy atoms of nuclease-H124L and its ternary complex. The backbone conformations of residues in regular secondary structural elements are defined better than those in turn and loop regions (Figs. 4A and 5A), which show slightly larger ⟨rmsd⟩ values. The pairwise rmsd values for the φ and ψ angles in the two structures are presented in Figs. 4D,E and 5D,E. The backbone torsion angles of the structures within each family are very similar, with more than 80% of the residues showing rmsd values less than 10°. Excluding the Pro[42]–Glu[57] segment and the termini, the average angular rmsd values for the φ and ψ angles in nuclease-H124L are 9 ± 4° and 12 ± 16°, respectively, whereas those of the ternary complex are 9 ± 4° and 10 ± 4°, respectively.

The stereochemical quality of the backbone coordinates of the two families of structures was analyzed using the program PROCHECK (Laskowski et al., 1996). 96.4 ± 0.2% and 96.6 ± 0.3% of residues in unligated nuclease and the ternary complex, respectively, are in favorable regions of torsion angle space. Except for Asn[138], all residues with φ/ψ angles outside allowed regions are in unstructured parts of the protein (N- and C-termini or the Pro[42]–Glu[57] loop). Asn[138] is the only residue consistently occupying unfavorable torsion angle space in all structures. Several hydrogen bonds appear to stabilize this unfavorable conformation.

Side-chain conformations

Side-chain heavy atom ⟨rmsd⟩ values are shown in Figs. 4B and 5B. For all heavy atoms in structured regions, the ⟨rmsd⟩ values are 0.91 (±0.07) Å and 0.83 (±0.05) Å for the unligated protein and the ternary complex (Table 4), respectively. Approximately 66% and 69% of the side chains of unligated nuclease and its ternary complex, respectively, exhibit ⟨rmsd⟩ values less than 1.2 Å. Most alanine, glycine, proline, and threonine residues, some aromatic rings, side chains of valine and leucine residues with unambiguous stereospecific assignments, and isoleucine side chains with several NOEs to neighboring residues show well-defined conformations. Resi-

TABLE 5
CLASSIFICATION OF β-TURNS

β-turn residue range	Turn type	β-turn residue range	Turn type
19–22	I	119–122	I
27–30	I'	137–140	II'
83–86	I	138–141	I
94–97	I'	139–142	I
115–118	VIa	140–143	I

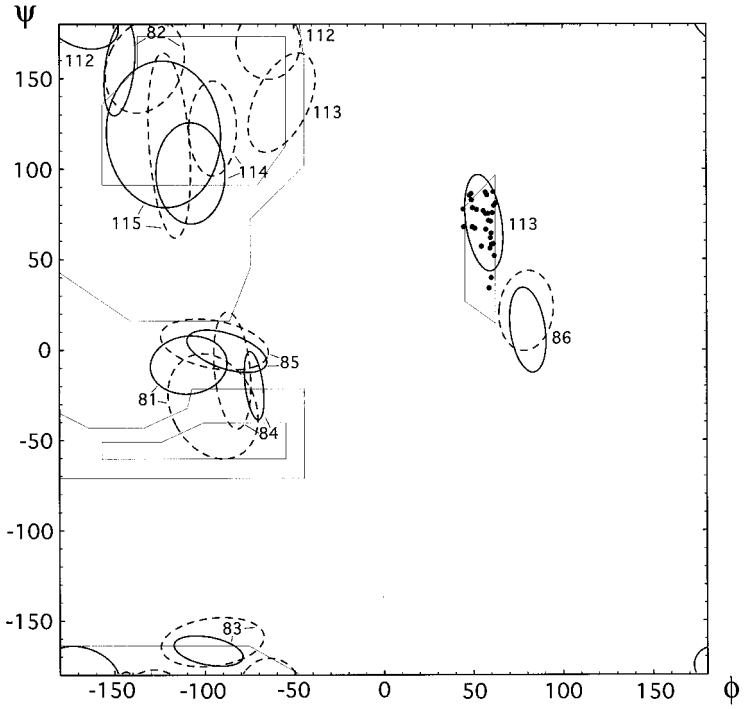

Fig. 9. Ramachandran plot (experimental ϕ and ψ torsion angles compared with conformational energy contours) showing the distribution of backbone ϕ and ψ torsion angles for residues Arg[81]–Glu[86] and Ala[112]–Tyr[115] among the 30 NMR solution structures of nuclease-H124L (dashed lines) and of the (nuclease-H124L)•pdTp•Ca^{2+} ternary complex (solid lines). The dots represent the backbone conformations of Tyr[113] in the 30 conformers that represent the structure of the (nuclease-H124L)•pdTp•Ca^{2+} ternary complex. Ellipses indicate the conformational space occupied by representative residues in the ensemble of conformers. These ellipses were determined from the covariance matrix of the ϕ and ψ angles such that the axes of the ellipse coincide with the eigenvectors of the covariance matrix and the lengths of the axes are equal to square roots of the corresponding eigenvalues. The ϕ/ψ covariance matrix was calculated for each residue by applying standard statistical procedures to the ϕ and ψ values derived from the ensemble of conformers representing each structure.

dues that are fairly inaccessible to solvent (less than 40% solvent surface accessibility) are among this group of residues with well-defined side-chain conformations. Almost all these residues are located in the α-helices or the β-barrel; some of them (Ala[12], Ile[15], Leu[25], Phe[34], Ile[72], Val[74], Phe[76], Tyr[91], and Ile[92]) are shown in Fig. 6. On the other hand, 14 and 7 residues in uncomplexed and complexed nuclease, respectively, display large ⟨rmsd⟩ values (>1.5 Å) and exhibit multiple χ^1 angles. Most of these are long, charged, fully solvent exposed side chains (e.g., lysine, arginine, glutamic acid, glutamine).

Details of the secondary and tertiary structures common to nuclease-H124L and its ternary complex

Representative elements of the secondary structure of the nuclease ternary complex are shown in Fig. 7. Most of the secondary structural elements derived from the NMR data have been described previously (Wang et al., 1990a,c,1992a,b) and are in agreement with the X-ray structures of nuclease-WT (Loll and Lattman, 1989; Hynes and Fox, 1991) and nuclease-H124L (Truckses et al., 1996). The refined solution structural models allow a more detailed analysis. Hydrogen bonding patterns and torsion angles in the final structures suggest that Glu[57]–Ala[69] form helix 1. NOEs suggest that helix 2 is formed by residues Met[98]–Ala[109]. However, only residues Met[98]–Arg[105] have torsion angles characteristic of a helix. The rest of the residues form a common C-terminal helix capping motif (Aurora et al., 1994): Gly[107] is in the left-handed α-helical conformation, and an i,i+3 hydrogen bond is deduced between Val[104] O and Gly[107] H^N. Also, an i,i+5 hydrogen bond was found between Leu[103] O and Leu[108] H^N. The same helix capping motif exists in helix 3 (Glu[122]–Glu[135]), with Lys[136] in the left-handed helical conformation. In this case, the i,i+3 hydrogen bond of the motif (between Lys[133] O and Lys[136] H^N) appears to be present in the structure of the complex, but not in that of unligated nuclease.

Five β-strands form a highly twisted β-barrel: (i) Lys[9]–Ala[17]; (ii) Thr[22]–Met[26]; (iii) Pro[31]–Arg[35]; (iv) Ile[72]–Phe[76]; and (v) Ala[90]–Tyr[93]. Strand 1 contains two β-bulges involving Ile[18], Asp[19] and Thr[22], and Ile[15], Lys[16] and Lys[24], respectively, allowing this strand to bend. In addition, Val[39]–Thr[41] and Ala[109]–Val[111] form a small antiparallel β-sheet.

Ten β-turns have been identified and classified (Table 5). Evidence for many of these turns came from NOE patterns (Wang et al., 1990c,1992b). However, a clear classification was only possible by inspection of the final

structures. The NMR data initially suggested that residues Ile[18]–Asp[21] form a turn; however, inspection of the structures showed that the β-turn is formed instead by Asp[19]–Thr[22]. The NOE pattern for these residues is misleading because of the β-bulge formed by Ile[18], Asp[19], and Thr[22]. As expected, Tyr[115]–Asn[118] form a type VI_a β-turn with the *cis* proline in the third position of the turn.

Nuclease contains three major loop regions. The conformation of the first loop, Pro[42]–Glu[57], is determined mainly by intraresidue and sequential NOE constraints in both structures and, therefore, is poorly defined with respect to the rest of the structure. This is reflected in large ⟨rmsd⟩ values for this loop (the highest approximately 7 Å) in both structures. Superposition of the backbone coordinates of this loop alone yields ⟨rmsd⟩ values for these residues of 1.96 (±0.38) Å and 1.82 (±0.45) Å, respectively, for nuclease-H124L and its ternary complex (Table 4). The sequential and short-range NOEs for this loop are not enough to determine its conformation as precisely as that for the rest of the protein. Nevertheless, in most of the conformers, its configuration can be described as that of an omega loop (Leszczynski and Rose, 1986). A comparison of the average conformation of this loop in the two structures suggests that binding of the inhibitor and Ca^{2+} causes rather subtle changes in its conformation and its orientation with respect to the rest of the structure, as has been observed in the crystal structures of nuclease-WT. The second loop, Asp[77]–Leu[89], consists of two well-defined lobes formed by Asp[77]–Arg[81] and Thr[82]–Leu[89]. The third loop, Ala[112]–Glu[122], is also well defined, and consists of an extended stretch followed by two β-turns.

Comparison of the NMR solution structures of nuclease-H124L and its ternary complex

Protein coordinates Superposition of the mean coordinates of nuclease-H124L and the ternary complex (Fig. 8A) reveals that the solution structures have identical secondary structural elements and that differences are localized to one loop. Tyr[113] has a dramatically different conformation in the two structures: it changes from an extended conformation in free nuclease-H124L to a left-handed α-helical conformation in the complexed protein (Fig. 8B). A significant shift (approximately 70°) is observed in the ϕ angle of the neighboring Ala[112]. These changes lead to reorientation of the side chain of Tyr[113], positioning it closer to Tyr[115] in the ternary complex as revealed by an NOE between $^1H^{\varepsilon}$ of Tyr[115] and $^1H^{\delta}$ of Tyr[113] (Wang et al., 1990b). Figure 9 illustrates the distribution of torsion angles among the two sets of 30 structures for residues Arg[81]–Gly[86] and Ala[112]–Tyr[115]. Complexation causes a decrease in torsion angle space for Arg[81]–Gly[86], which is reflected in the smaller size of the ovals in Fig. 9; quantitatively, it amounts to a decrease in the ⟨rmsd⟩ for backbone atoms from 0.59 to 0.43 Å. Also, the atom positions of the side chains of residues involved in intermolecular protein–pdTp constraints (Arg[35], Lys[84], Tyr[85], Arg[87], Tyr[113], and Tyr[115]) are defined more precisely in the complex than in unligated nuclease: the ⟨rmsd⟩ values for these side chains are 1.63 and 0.84 Å, respectively, in nuclease-H124L and its ternary complex. More detailed information on internal dynamics is needed to determine whether this greater precision of side chains in the ternary complex represents a real tightening of the structure or whether it is simply a consequence of the additional constraints observed for these side chains.

Hydrogen exchange Previous NMR studies showed that overall amide proton exchange is more rapid in the free protein than in the ternary complex (Loh et al., 1993). These differences are not reflected in observable differences in overall backbone rmsd values (Table 4), suggesting that the amide proton exchange results report on different time scales of dynamics than can be detected in these time-averaged coordinates. The amide exchange results also indicated that a local opening occurs in the C-terminal half of the protein (helices 2 and 3 and the turn and extended segments between them) and that this dynamic process is eliminated in the ternary complex. No evidence for this difference in local dynamics is evident from the calculated structural models.

Chemical shifts Comparison of the NMR resonances ($^1H^N$, ^{15}N, $^{13}C^{\alpha}$, $^{13}C'$, $^1H^{\alpha}$ as well as $^1H^{\beta}$) for the two proteins shows that the largest chemical shift changes upon ternary complex formation occur in two regions: Ala[109]–Tyr[115] and Arg[35]–Thr[41]. Smaller changes occur mainly for the $^1H^N$ and ^{15}N resonances of residues Gly[20]–Lys[24] and Lys[48]–Gly[55]. Considering that the most significant conformational differences are observed for Tyr[113], it is not surprising that the largest chemical shift differences occur in the vicinity of this residue. According to the crystal structure, Ca^{2+} is coordinated by Asp[21], Asp[40], and Thr[41]. A change in the chemical environment caused by Ca^{2+} can explain the chemical shift differences observed for these residues, whose conformations are not appreciably different in the two structures. Both Arg[35] and Arg[87] are thought to hydrogen bond to the 5'-phosphate of pdTp; however, significant chemical shift changes are only observed for Arg[35]. Several other residues exhibit chemical shift changes that can be accounted for neither by local interactions with pdTp or Ca^{2+} nor by observable conformational changes. They may reflect subtle conformational differences in the ensembles of structures representing the unligated nuclease and its ternary complex that are not evident in the conformational models.

Evidence for a minor conformation In addition to the strong resonances, weak minor peaks have been observed for the side-chain atoms of residues Val[74] (not shown), Phe[76], Tyr[91], His[121] (not shown), and Trp[140] (Fig. 10). These minor peaks are present in spectra of the free protein but not the binary or ternary complex with pdTp.

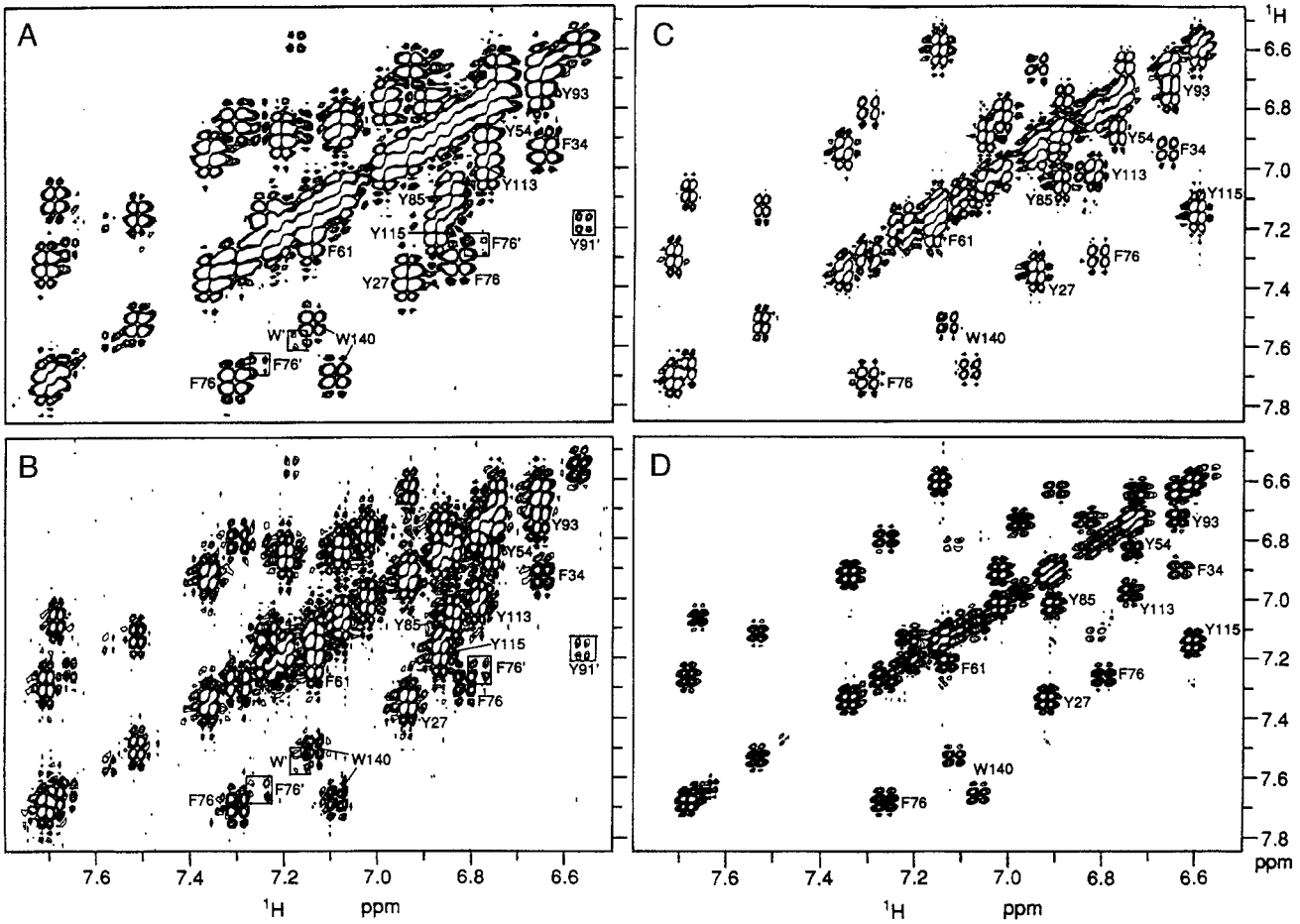

Fig. 10. Aromatic region of a 2D ^{1}H DQF-COSY spectrum of nuclease-H124L at natural isotopic abundance: (A) uncomplexed nuclease-H124L (Wang et al., 1992a); (B) nuclease•Ca^{2+} binary complex; (C) nuclease•pdTp binary complex; (D) nuclease•pdTp•Ca^{2+} ternary complex (Wang et al., 1990c). Assigned cross peaks are labeled with the one-letter amino acid code and residue number. Cross peaks assigned to the minor conformation are boxed and labeled with primed numbers.

Residues Val[74], Phe[76], and Tyr[91] are located relatively near Pro[117]. Thus, it is assumed that the extra peaks arise from the minor population of protein molecules in which the Lys[116]–Pro[117] peptide bond is in the *trans* configuration; the population of this minor species is about 10% in uncomplexed nuclease-H124L but is close to 0% in the ternary complex (Alexandrescu et al., 1989). Previous studies have shown that mutations at nearby residues can change the *cis*/*trans* equilibrium of this peptide bond dramatically (Hinck et al., 1996). Thus, it is not surprising that the conformation of these residues is sensitive to the configuration of the Lys[116]–Pro[117] peptide bond. The presence of minor peaks for Trp[140], which is situated near the C-terminus of the protein and far from the Lys[116]–Pro[117] peptide bond, suggests that longer range structural changes are coupled to the configurational state of the Lys[116]–Pro[117] peptide bond.

Comparisons with available X-ray structures

Overall protein fold The family of NMR-derived structural models for the free protein was compared with the crystal structure model of nuclease-H124L (Truckses et al., 1996). Similarly, the family of structural models for the ternary complex of nuclease-H124L was compared with the X-ray structure of the nuclease-WT ternary complex (Loll and Lattman, 1989). Superpositions of the respective structures are shown in Fig. 3. The secondary and tertiary structures are basically identical in both cases, except for the following differences in helix 1 and at the C-terminus. Tyr[54]–Pro[56] form the N-terminus of helix 1 in the crystal structures, but have a poorly defined conformation in both solution structures. They seem part of the flexible loop that precedes this helix. Ser[141] is the last residue at the protein C-terminus defined by the X-ray diffraction data. In contrast, NOE distance constraints were obtained up to Asp[143], leading to a well-defined conformation up to Trp[140] and to an imprecise, but still helical, conformation for the next two residues.

In comparing the X-ray structures with the respective experimental NMR constraints, it was found that the X-ray structure of nuclease-H124L (Truckses et al., 1996) violates 24 of 1968 NOE constraints (for residues 7

TABLE 6
VIOLATIONS OF EXPERIMENTAL NOE CONSTRAINTS IN THE CRYSTAL STRUCTURE[a]

Atoms assigned to NOE		NMR exp. distance (upper limit) (Å)	Measured distance (Å)	Difference (Å)
Nuclease-H124L				
Glu^{10} H^N	Glu^{10} $H^{\gamma 2}$	3.10 (3.5)	4.09	0.99
Glu^{10} H^N	Lys^{9} $H^{\epsilon *}$	5.50 (6.5)	6.87	1.37
Ile^{18} H^N	Ile^{18} $H^{\gamma 11}$	2.70 (3.5)	3.90	1.20
Ile^{18} H^{α}	Ile^{18} $H^{\gamma 11}$	3.10 (3.5)	3.74	0.64
Ile^{18} H^{α}	Ile^{18} $H^{\gamma 12}$	2.30 (2.7)	3.27	0.97
Phe^{34} $H^{\epsilon 1}$	Met^{32} $H^{\beta 2}$	2.60 (2.7)	3.97	1.37
Lys^{63} H^{α}	Lys^{63} $H^{\gamma 2}$	2.30 (2.7)	3.30	1.00
Met^{65} H^N	Phe^{61} H^{α}	3.40 (3.5)	4.11	0.71
Met^{65} H^{α}	Asn^{68} $H^{\beta 2}$	2.90 (3.5)	3.86	0.96
Asn^{68} H^N	Asn^{68} $H^{\delta 22}$	3.40 (3.5)	4.74	1.34
Asn^{68} $H^{\delta 21}$	Lys^{64} H^{α}	4.20 (5.3)	5.58	1.38
Ala^{69} H^N	Met^{65} H^{α}	3.30 (3.5)	5.06	1.76
Lys^{84} H^N	Lys^{84} $H^{\gamma 2}$	2.90 (3.5)	4.37	1.47
Arg^{87} H^N	Arg^{87} $H^{\delta *}$	2.90 (3.5)	4.77	1.87
Lys^{97} H^N	Asp^{95} $H^{\beta 2}$	3.40 (3.5)	3.83	0.43
Lys^{97} H^N	Lys^{97} $H^{\gamma 1}$	2.80 (3.5)	3.77	0.97
Lys^{110} H^N	Ile^{139} $H^{\delta 1 *}$	6.00 (6.5)	7.00	1.00
Asn^{119} $H^{\delta 22}$	Asn^{114} $H^{\gamma *}$	4.50 (5.3)	5.91	1.41
Ser^{128} H^N	Leu^{124} $H^{\delta 2 *}$	5.80 (6.5)	7.08	1.28
Glu^{135} H^N	Leu^{137} $H^{\beta 1}$	5.50 (6.5)	6.71	1.21
Lys^{136} H^N	Trp^{140} $H^{\beta 1}$	3.30 (3.5)	4.26	0.96
Ile^{139} H^N	Ile^{139} $H^{\gamma 1 *}$	2.80 (3.5)	3.88	1.08
Trp^{140} $H^{\delta 1}$	Leu^{137} $H^{\delta 1 *}$	5.00 (5.3)	5.75	0.75
Trp^{140} $H^{\zeta 2}$	Lys^{133} $H^{\delta *}$	4.70 (5.3)	5.83	1.13
Nuclease-H124L ternary complex				
Leu^{7} H^N	Leu^{7} $H^{\beta *}$	3.40 (3.5)	3.79	0.39
His^{8} H^N	Leu^{7} $H^{\delta 1 *}$	4.50 (5.3)	5.68	1.18
His^{8} H^N	His^{8} $H^{\delta 2}$	4.50 (5.3)	5.66	1.16
Thr^{13} H^N	Leu^{25} $H^{\beta 2}$	3.40 (3.5)	4.86	1.46
His^{46} H^{α}	Pro^{47} $H^{\delta 1}$	3.00 (3.5)	3.77	0.77
His^{46} $H^{\delta 2}$	His^{46} H^{α}	3.40 (3.5)	4.18	0.78
Lys^{64} H^N	Lys^{64} $H^{\delta 1}$	2.90 (3.5)	3.76	0.86
Val^{66} H^N	Thr^{62} H^{α}	3.40 (3.5)	3.93	0.53
Asn^{68} H^N	Glu^{67} $H^{\beta 1}$	3.20 (3.5)	3.84	0.64
Asn^{68} $H^{\delta 21}$	Lys^{64} $H^{\gamma 2}$	4.40 (5.3)	6.48	2.08
Phe^{76} $H^{\epsilon 2}$	Phe^{34} H^{ζ}	3.40 (3.5)	4.22	0.82
Ala^{90} H^N	Leu^{89} $H^{\beta 1}$	3.40 (3.5)	3.80	0.40
Asn^{100} H^N	Met^{98} $H^{\gamma 1}$	3.00 (3.5)	3.81	0.81
Leu^{108} H^N	Leu^{103} $H^{\beta 2}$	3.50 (5.3)	5.52	2.02
Ala^{109} H^N	Leu^{103} $H^{\beta 2}$	3.90 (5.3)	5.52	1.62
Lys^{133} H^N	Lys^{133} $H^{\delta 2}$	5.00 (5.3)	5.51	0.51
Asn^{138} $H^{\delta 22}$	Gln^{106} $H^{\gamma 1}$	4.00 (5.3)	5.68	1.68
Asn^{138} $H^{\delta 22}$	Leu^{137} H^{γ}	5.00 (5.3)	5.72	0.72
Trp^{140} $H^{\delta 1}$	Ile^{139} $H^{\delta 1 *}$	4.70 (5.3)	6.90	2.2
Trp^{140} $H^{\zeta 2}$	Lys^{133} $H^{\gamma *}$	4.40 (5.3)	5.86	1.46

[a] Experimental distances were derived from NOE data. Some experimental distances have been adjusted to include pseudoatoms (*). The measured distances are for the crystal structures; in the case of free protein, distances for the crystal structure of nuclease-H124L (Truckses et al., 1996) are listed, whereas distances for the crystal structure of the (nuclease-H124L)•pdTp•Ca^{2+} complex (Loll and Lattman, 1989) are listed for the ternary complex.

through 141) by more than 0.2 Å (Table 6), but satisfies all the torsion angle constraints. Most of the violated NOE constraints are between side-chain atoms or between side-chain and backbone atoms. However, two of them are between backbone hydrogens; these involve residues in the C-terminal half of helix 1 (a 0.71 Å violation in the distance between H^N of Met^{65} and H^{α} of Phe^{61} and a 1.76 Å violation in the distance between H^N of Val^{69} and H^{α} of Thr^{65}). In the case of the ternary complex, the X-ray structure of nuclease-WT (Loll and Lattman, 1989) violates 20 of 1970 distance constraints (for residues 7 through 141) by more than 0.2 Å (Table 6) and all the torsion angle constraints are satisfied. Only one of the violated NOE constraints is between backbone hydrogens (a 0.4 Å violation in the distance between H^N of Val^{66} and H^{α} of Thr^{62}). As in the free protein, this violation is located in helix 1; nevertheless, in both cases the conformation of this helix is very similar in the solution and crystal structures. The only significant difference is at the C-terminus of this helix in the free protein. The conformations of Asn^{68} and Val^{69} in the crystal structure are slightly different, as described below, resulting in a geometry for the last helical hydrogen bond (between H^N of Val^{69} and H^{α} of Thr^{65}) that is more strained in the crystal structure than in the solution structure.

Backbone atom positions Residue-by-residue comparisons of the solution and crystal structures are shown in Figs. 11 and 12. The structured regions of the conformers derived from NMR data (residues 8–41 and 58–140) superimpose on the X-ray structure of nuclease and its ternary complex, respectively, with an rmsd for backbone coordinates of 0.6 (±0.2) Å in each case. This global correspondence is reflected in the similarity of the local conformation throughout the structured parts of the protein. As shown in Figs. 11C,D and 12C,D, the ensemble of ϕ and ψ angles in most cases includes the corresponding value in the X-ray structure. The only significant exceptions are the ϕ and ψ values for Asn^{68} and Ala^{69} in the free protein which do not include the X-ray values, which is consistent with the significant violation of the NOE between H^N of Ala^{69} and H^{α} of Met^{65} (Table 6). Excluding the flexible loop, the average torsion angle deviations between the X-ray and solution structures are 13 (±7)° for ϕ and 15 (±9)° for ψ in the free protein and 11 (±6)° for ϕ and 13 (±6)° for ψ in the ternary complex.

As stated above, the conformation of the flexible loop (Pro^{42}–Glu^{57}) is not defined precisely in either the solution or crystal structures. However, the position of the loop in the X-ray structures is clearly outside the family of conformers that represent this loop in the NMR structure. Among the small number of experimental constraints for this loop, few are violated by the crystal structures. This indicates that the calculated family of NMR conformers does not sample fully the conformational space for these loop residues allowed by the NMR constraints alone; this result may be explained by a high empirical energy for these residues in the crystal structure.

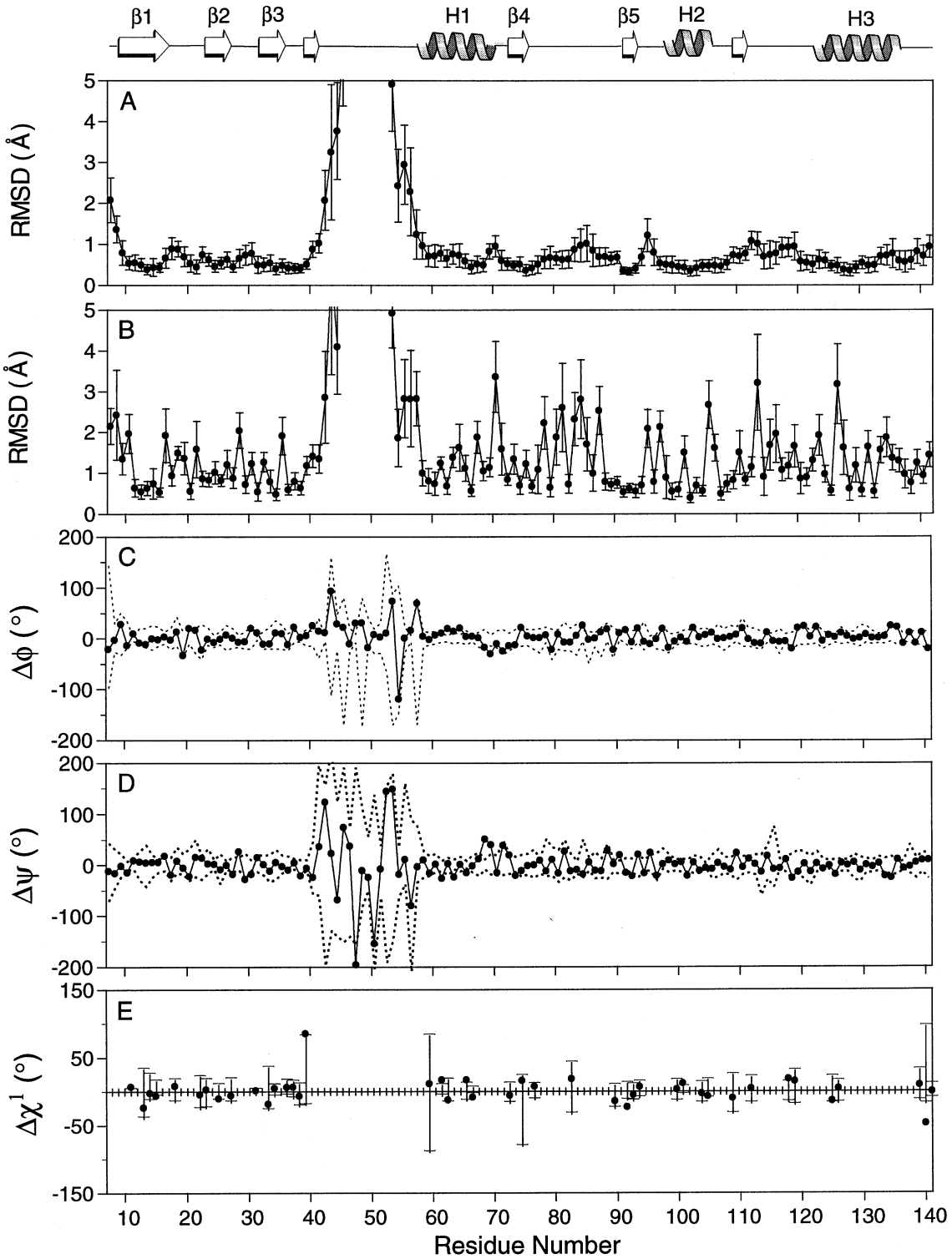

Fig. 11. (A) Rmsd values of heavy-atom backbone coordinates for the 30 structures of nuclease-H124L relative to the 1.7 Å X-ray structure (Truckses et al., 1996). Residues in structured regions were used for the superposition. (B) Rmsd values of all heavy-atom coordinates for every residue among the 30 structures relative to the X-ray structure. Comparison of (C) ϕ and (D) ψ angles in the NMR and X-ray structures. The dotted lines show the maximum (top) and minimum (bottom) difference from the average angle among the 30 NMR structures. The solid line indicates the difference between the angle in the X-ray structure and the average angle among the NMR structures. (E) Comparison of χ^1 angles in the family of NMR structures and the X-ray structure. Only residues that have heavy-atom coordinate rmsd values from the average NMR coordinates less than or equal to 0.7 Å are shown. Vertical lines display the maximum and minimum deviations of χ^1 from the average value among the NMR structures and dots indicate the difference between the X-ray and the average NMR χ^1 angles. The large deviations from the average χ^1 angle, indicated for some residues, are due to outliers. Small vertical lines are shown to aid in identification of the residues. In all these graphs, Ala^1–Lys^6 and Glu^{142}–Gln^{149} are not shown as these residues do not have defined X-ray coordinates.

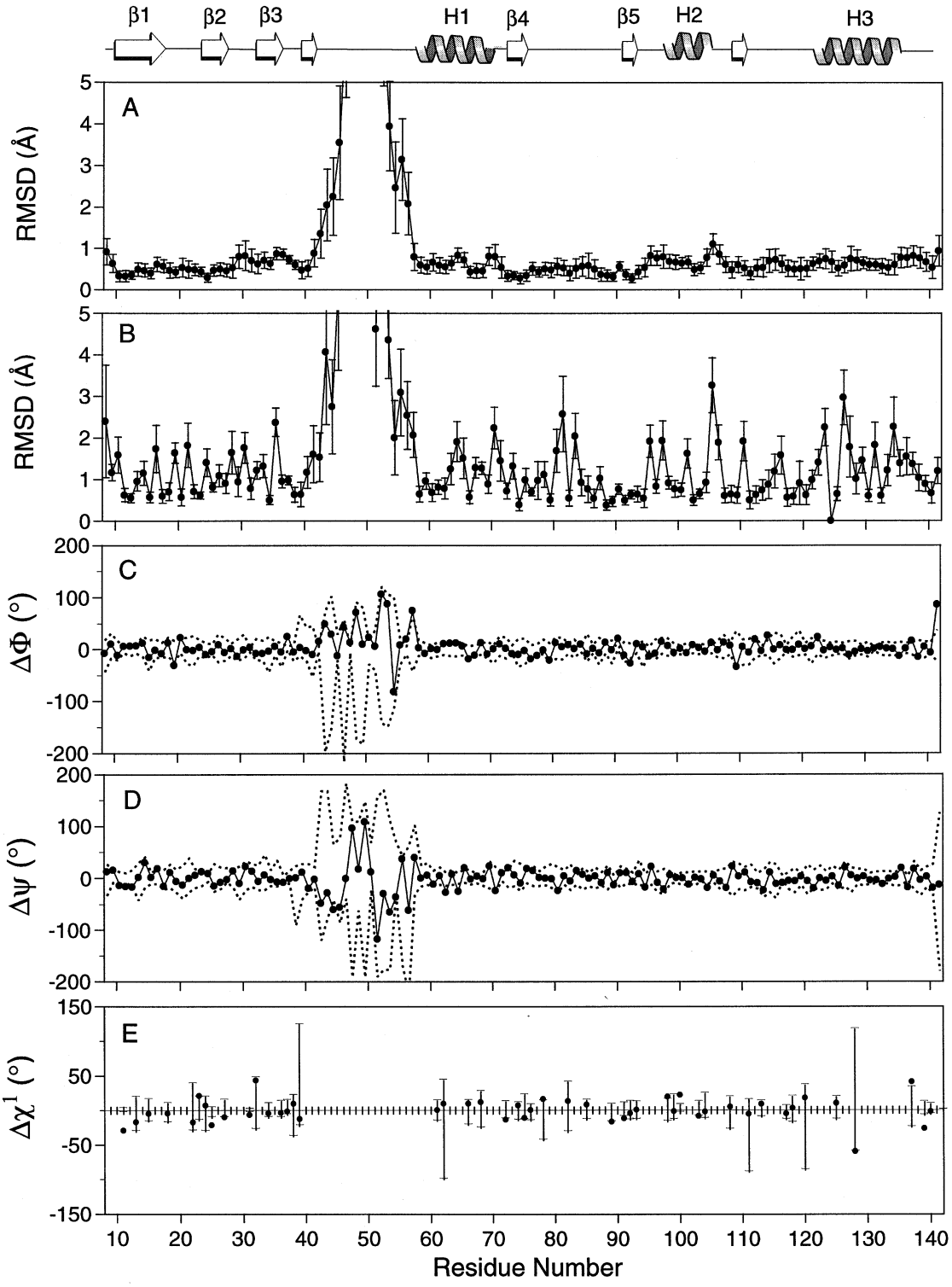

Fig. 12. (A) Rmsd values of heavy-atom backbone coordinates for the 30 structures of nuclease-H124L relative to the 1.65 Å X-ray structure of the (nuclease-WT)•pdTp•Ca^{2+} ternary complex (Loll and Lattman, 1989). Residues in structured regions were used for the superposition. For an explanation of (B)–(E), see the caption to Fig. 11.

Hydrogen bonding According to geometric criteria (Baker and Hubbard, 1984), most of the hydrogen bonds observed in the crystal structures between backbone atoms are also present in the corresponding family of solution structures. By contrast, hydrogen bonds observed in the crystal structures involving side chains are not present in most of the solution structural models. The NMR structures would support the presence of some of these hydro-

TABLE 7
NUMBER OF THE 30 STRUCTURES CONTAINING CERTAIN HYDROGEN BONDS

Donor	Acceptor	Nuclease-H124L[a]	Nuclease-H124L ternary complex[a]
Main chain to side chain hydrogen bonds observed in the X-ray structures			
Arg^{35} $N^{\eta 1}$	Leu^{36} O	0 (5)	1 (1)
Arg^{35} $N^{\eta 1}$	Val^{39} O	1 (1)	0 (1)
Arg^{35} $N^{\eta 2}$	Val^{39} O	2 (3)	1 (1)
Thr^{62} $O^{\gamma 1}$	Gly^{20} O	5 (12)	3 (7)
Lys^{70} N	Asp^{95} $O^{\delta 1}$	0 (4)	11 (17)
Lys^{70} N	Asp^{95} $O^{\delta 2}$	0 (0)	0 (3)
Lys^{71} N	Asp^{95} $O^{\delta 2}$	0 (1)	0 (2)
Lys^{78} N	Asp^{77} $O^{\delta 2}$	2 (2)	4 (5)
Gly^{79} N	Asn^{118} $O^{\delta 1}$	3 (10)	30 (30)
Tyr^{85} N	Asp^{83} $O^{\delta 1}$	5 (5)	4 (4)
Arg^{87} N	Asp^{83} $O^{\delta 1}$	5 (5)	5 (5)
Ile^{92} N	Asn^{100} $O^{\delta 1}$	17 (25)	1 (18)
Asn^{100} $N^{\delta 2}$	Leu^{37} O	8 (27)	4 (4)
Val^{111} N	Glu^{129} $O^{\epsilon 1}$	5 (16)	0 (0)
Asn^{118} $N^{\delta 2}$	Gln^{80} O	3 (7)	1 (15)
Thr^{120} N	Asp^{77} $O^{\delta 1}$	5 (12)	11 (24)
His^{121} N	Tyr^{91} O^{η}	2 (10)	1 (15)
Asn^{138} $N^{\delta 2}$	Gln^{106} O	8 (21)	22 (28)
Ser^{141} O^{γ}	Asn^{138} O	0 (1)	1 (6)
Main chain to side chain hydrogen bonds not observed in the X-ray structures			
Thr^{62} $O^{\gamma 1}$	Ala^{58} O	2 (7)	0 (1)
Asn^{68} $N^{\delta 2}$	Lys^{64} O	10 (14)	5 (15)
Asn^{119} N	Asp^{77} $O^{\delta 2}$	0 (3)	0 (9)
Ser^{128} O^{γ}	Leu^{124} O	0 (2)	4 (6)
Ser^{141} O^{γ}	Lys^{136} O	2 (8)	3 (7)
Side chain to side chain hydrogen bonds observed in the X-ray structures			
Thr^{22} $O^{\gamma 1}$	Asp^{21} $O^{\delta 2}$	3 (6)	0 (0)
Tyr^{27} O^{η}	Glu^{10} $O^{\epsilon 2}$	1 (4)	2 (5)
Arg^{35} $N^{\eta 2}$	Asp^{40} $O^{\delta 1}$	2 (5)	1 (2)
Lys^{63} N^{ζ}	Glu^{67} $O^{\epsilon 2}$	1 (4)	2 (4)
Tyr^{85} O^{η}	Lys^{84} N^{ζ}	0 (0)	6 (9)
Arg^{87} N^{ϵ}	Asp^{83} $O^{\delta 2}$	0 (0)	0 (2)
Arg^{87} $N^{\eta 1}$	Asp^{83} $O^{\delta 2}$	0 (0)	2 (4)
Tyr^{91} O^{η}	Asp^{77} $O^{\delta 1}$	3 (5)	3 (7)
Tyr^{93} O^{η}	Glu^{75} $O^{\epsilon 2}$	3 (8)	2 (10)
Arg^{105} $N^{\eta 1}$	Glu^{135} $O^{\epsilon 1}$	0 (0)	0 (2)
Arg^{105} $N^{\eta 2}$	Glu^{135} $O^{\epsilon 2}$	1 (1)	2 (2)
Thr^{120} $O^{\gamma 1}$	Asp^{77} $O^{\delta 2}$	1 (1)	7 (10)
His^{121} $N^{\epsilon 2}$	Glu^{75} $O^{\epsilon 2}$	4 (11)	5 (17)
Arg^{126} N^{ϵ}	Glu^{122} $O^{\epsilon 1}$	1 (2)	0 (0)
Arg^{126} $N^{\eta 2}$	Glu^{122} $O^{\epsilon 1}$	1 (1)	0 (2)
Ser^{128} O^{γ}	Glu^{101} $O^{\epsilon 2}$	2 (3)	0 (1)
Gln^{131} $N^{\epsilon 2}$	Glu^{135} $O^{\epsilon 1}$	0 (1)	1 (3)

[a] Strict (loose) criteria for hydrogen bonding. Minimum angles: donor–proton–acceptor 110.0° (90.0°); proton–acceptor–carbon 90.0° (90.0°); donor–acceptor–carbon 90.0° (90.0°). Maximum distances: donor–acceptor 3.9 Å (3.9 Å); proton–acceptor 2.5 Å (3.0 Å).

gen bonds if less stringent geometric criteria were applied (Table 7); however, available hydrogen exchange data (Loh et al., 1993) lend no support to the existence of these backbone–side-chain hydrogen bonds in solution. By contrast, a few backbone–side-chain hydrogen bonds not observed in the X-ray structures appear to be present in the NMR structure (Table 7).

Conformation and mobility of side chains The average rmsd between the NMR and X-ray structures for all heavy atoms in structured regions is 1.2 (±0.7) Å and 1.1 (±0.6) Å, respectively, for free and complexed nuclease. Residues that are buried in the solution structure (i.e., have ≤20% solvent exposure in all 30 conformers) have average heavy-atom rmsd values, with respect to coordinates of the X-ray structure, of 0.8 (±0.3) Å (0.9 Å for side chains only) and 0.8 (±0.4) Å (0.9 Å for side chains only), respectively, for the free and complexed protein. These side chains have well-defined conformations in the NMR structures that are similar to those reported for the X-ray structures. Most of the side chains with ⟨rmsd⟩

values ≤0.7 Å for all heavy atoms in the family of solution structure conformers have χ^1 angles identical, within experimental error, to those in the X-ray structures (Figs. 11E and 12E). However, although this analysis suggests good general agreement between the conformations of ordered side chains in the solution and crystal environments, the positions of several side chains in the crystal appear to be stabilized by hydrogen bonds that are not observed in solution (Table 7). For those side chains whose positions are well defined in both the solution and crystal structures (viz., Thr^{22}, Tyr^{27}, Thr^{62}, Glu^{75}, Tyr^{85} (complex only), Tyr^{91}, Tyr^{93}, Asp^{100}, Thr^{120}, and Ser^{128}), the differences in hydrogen bonding can be interpreted as indicating the existence of small conformational differences in the two environments. A second class of residues has side chains that appear to be rigid in the crystal but mobile in solution (viz., Glu^{10}, Asp^{21}, Arg^{35}, Asp^{40}, Lys^{63}, Glu^{67}, Asp^{77}, Asp^{83}, Tyr^{85} (free protein only), Arg^{87}, Asp^{95}, Glu^{101}, Arg^{105}, His^{121}, Glu^{122}, Arg^{126}, Glu^{129}, Gln^{131}, Glu^{135}, and Ser^{141}). Nine of these residues (Lys^{63}, Glu^{67}, Lys^{84}, Tyr^{85}, Asp^{95}, Arg^{105}, Arg^{126}, Gln^{131}, and Glu^{135}) are more than 40% solvent exposed. Surface residues certainly are less ordered in solution than in the crystal, but some of the apparent disorder may result simply from the low number of structural constraints for surface residues that lack nearby groups or from the quenching of NOEs by internal motions. The other residues (Arg^{35}, Asp^{40}, Asp^{77}, Asp^{83}, Arg^{87}, Glu^{101}, His^{121}, Glu^{122}, Glu^{129}, and Ser^{141}) are less than 40% solvent exposed (i.e., more buried). One can be more confident that these residues are less ordered in solution than in the crystal.

Additional evidence for the existence of small, but real, differences in side-chain conformation in the solution and crystal environments comes from the analysis of NOEs that are incompatible with the crystal structures (Table 6). Most of the side chains whose conformations violate NOE constraints have relatively low thermal factors in the models derived from X-ray data, indicating that the conformations of these residues are ordered in the crystal.

Conclusions

Most of the structural features observed in the NMR solution structures of staphylococcal nuclease-H124L and the (nuclease-H124L)•pdTp•Ca^{2+} ternary complex are identical, within experimental error, to those present in the respective X-ray structures. The similarities include the overall fold, the positions of β-bulges, the unfavorable torsion angle space observed for Asn^{138}, and the C-terminal helix capping motifs of helices 2 and 3. The N- and C-termini of the solution structure are disordered, in agreement with the lack of electron density for these residues in the X-ray structures. In each of the NMR structures (nuclease-H124L and its ternary complex), the least structured stretch was Pro^{42}–Glu^{57}; this mobile loop contains the functionally important Ca^{2+} binding site. This result is consistent with the high B-factors observed for Pro^{42}–Tyr^{54} in the corresponding X-ray structures; however, the disordered loop extends to Glu^{57} in the NMR structures, whereas Gly^{55} and Pro^{56} form the C-terminus of helix 1 in the X-ray structures. Ca^{2+} and inhibitor binding cause a dramatic change in the conformation of Tyr^{113} in solution (from an extended conformation to a left-handed α-helical conformation), in agreement with the crystal structures. In addition, complexation appears to stabilize the conformation of residues Arg^{81}–Gly^{86} and the positions of the side chains that bind the nucleotide.

Acknowledgements

This research was supported by Grant GM35976 from the U.S. National Institutes of Health (NIH). NMR studies were carried out at the National Magnetic Resonance Facility at Madison, whose operation is subsidized by Grant RR02301 from the NIH National Center for Research Resources and whose instrumentation was purchased with funds from the U.S. National Science Foundation, the University of Wisconsin-Madison, the NIH, and the U.S. Department of Agriculture. We thank Prof. Masatsune Kainosho of Tokyo Metropolitan University for providing samples of chiral ^{13}C-labeled leucine and valine, Dr. Andrew Hinck for preparing the protein samples containing these labeled amino acids, Marvin M. Goodman and Susan M. Geer at Eastman Kodak for providing the HMQCJFIT program to aid the analysis of the HMQC-J data, Prof. Axel Brünger of Yale University for advice in using the X-PLOR software package, and Dr. Bin Xia who helped prepare some of the figures.

References

Alexandrescu, A.T., Ulrich, E.L. and Markley, J.L. (1989) *Biochemistry*, **28**, 204–211.

Arseniev, A., Schultze, P., Wörgötter, E., Braun, W., Wagner, G., Vasák, M., Kägi, J.H.R. and Wüthrich, K. (1988) *J. Mol. Biol.*, **201**, 637–657.

Aurora, R., Srinivasan, R. and Rose, G.D. (1994) *Science*, **264**, 1126–1130.

Baker, E.N. and Hubbard, R.E. (1984) *Prog. Biophys. Mol. Biol.*, **44**, 97–179.

Baldisseri, D.M., Torchia, D.A., Poole, L.B. and Gerlt, J.A. (1991) *Biochemistry*, **30**, 3628–3633.

Bax, A., Clore, G.M., Driscoll, P.C., Gronenborn, A.M., Ikura, M. and Kay, L.E. (1990) *J. Magn. Reson.*, **87**, 620–627.

Bax, A. and Pochapsky, S.S. (1992) *J. Magn. Reson.*, **99**, 638–643.

Brünger, A.T. (1992) X-PLOR Version 3.1 Manual, Yale University, New Haven, CT, U.S.A.

Chothia, C. (1975) *Nature*, **254**, 304–308.

Chylla, R.A. and Markley, J.L. (1995) *J. Biomol. NMR*, **5**, 245–258.

Cotton, F.A., Hazen Jr., E.E. and Legg, M.J. (1979) *Proc. Natl. Acad. Sci. USA*, **76**, 2551–2555.

Forman-Kay, J.D., Gronenborn, A.M., Kay, L.E., Wingfield, P.T. and Clore, G.M. (1990) *Biochemistry*, **29**, 1566–1572.

Gondol, D. and Van Binst (1986) *Biopolymers*, **25**, 977–983.
Goodgame, M.M. and Geer, S.M. (1993) *J. Magn. Reson.*, **A102**, 246–248.
Griesinger, C., Sørensen, O.W. and Ernst, R.R. (1982) *J. Am. Chem. Soc.*, **104**, 6800–6802.
Grzesiek, S. and Bax, A. (1992) *J. Magn. Reson.*, **96**, 432–440.
Hinck, A.P., Eberhardt, E.S. and Markley, J.L. (1993) *Biochemistry*, **32**, 11810–11818.
Hinck, A.P., Walkenhorst, W.F., Truckses, D.M. and Markley, J.L. (1996) In *Biological NMR Spectroscopy* (Eds., Markley, J.L. and Opella, S.J.), Oxford University Press, New York, NY, U.S.A., pp. 111–138.
Hodel, A., Kautz, R.A., Jacobs, M.D. and Fox, R.O. (1993) *Protein Sci.*, **2**, 838–850.
Hodel, A., Kautz, R.A. and Fox, R.O. (1995) *Protein Sci.*, **4**, 484–495.
Hyberts, S.G., Marki, W. and Wagner, G. (1987) *EMBO J.*, **164**, 625–635.
Hynes, T.R., Kautz, R.A., Goodman, M.A., Gill, J.F. and Fox, R.O. (1989) *Nature*, **339**, 73–76.
Hynes, T.R. and Fox, R.O. (1991) *Proteins Struct. Funct. Genet.*, **10**, 92–105.
Hynes, T.R., Hodel, A. and Fox, R.O. (1994) *Biochemistry*, **33**, 5021–5030.
Ikura, M., Bax, A., Clore, G.M. and Gronenborn, A.M. (1990) *J. Am. Chem. Soc.*, **112**, 9020–9022.
Jeener, J., Meier, B.H., Bachmann, P. and Ernst, R.R. (1979) *J. Chem. Phys.*, **71**, 4546–4553.
Kay, L.E. and Bax, A. (1990) *J. Magn. Reson.*, **86**, 110–126.
Kay, L.E., Wittekind, M., McCoy, M.A., Friedrichs, M.S. and Mueller, L. (1992) *J. Magn. Reson.*, **98**, 443–450.
Kay, L.E., Xu, G.-Y., Singer, A.U., Muhandiram, D.R. and Forman-Kay, J.D. (1993) *J. Magn. Reson.*, **B101**, 333–337.
Keefe, L.J., Quirk, S., Gittis, A., Sondek, J. and Lattman, E.E. (1993) *Proc. Natl. Acad. Sci. USA*, **90**, 3275–3279.
Kline, A.D., Braun, W. and Wüthrich, K. (1988) *J. Mol. Biol.*, **204**, 675–724.
Laskowski, R.A., Rullmann, J.A.C., MacArthur, M.W., Kaptein, R. and Thornton, J.M. (1996) *J. Biomol. NMR*, **8**, 477–486.
Lee, B. and Richards, F.M. (1971) *J. Mol. Biol.*, **55**, 379–400.
Leszczynski, J.F. and Rose, G.D. (1986) *Science*, **234**, 849–855.
Libson, A., Gittis, A. and Lattman, E.E. (1994) *Biochemistry*, **33**, 8007–8016.
Loh, S.N., Prehoda, K.E., Wang, J. and Markley, J.L. (1993) *Biochemistry*, **32**, 11022–11028.
Loll, P.A. and Lattman, E.E. (1989) *Proteins Struct. Funct. Genet.*, **5**, 183–201.
Marion, D. and Wüthrich, K. (1983) *Biochem. Biophys. Res. Commun.*, **113**, 967–974.
Marion, D., Ikura, M. and Bax, A. (1989a) *J. Magn. Reson.*, **84**, 425–430.
Marion, D., Ikura, M., Tschudin, R. and Bax, A. (1989b) *J. Magn. Reson.*, **85**, 393–399.
Marion, D., Kay, L.E., Sparks, S.W., Torchia, D.A. and Bax, A. (1989c) *J. Am. Chem. Soc.*, **111**, 1515–1517.
McDonald, I.K. and Thornton, J.M. (1994) *J. Mol. Biol.*, **238**, 777–793.
Momany, F.A., McGuire, R.F., Burgess, A.W. and Scheraga, H.A. (1975) *J. Phys. Chem.*, **79**, 2361–2381.
Mooberry, E.S., Abildgaard, F. and Markley, J.L. (1994) *Methods Enzymol.*, **239**, 247–256.
Nilges, M., Clore, G.M. and Gronenborn, A.M. (1988) *FEBS Lett.*, **229**, 317–324.
Nilges, M., Kuszewski, J. and Brünger, A.T. (1991) In *Computational Aspects of the Study of Biological Macromolecules by NMR* (Ed., Hoch, J.C.), Plenum, New York, NY, U.S.A.
Pardi, A., Billeter, M. and Wüthrich, K. (1984) *J. Mol. Biol.*, **180**, 741–751.
Rance, M., Sørensen, O.W., Bodenhausen, G., Wagner, G., Ernst, R.R. and Wüthrich, K. (1983) *Biochem. Biophys. Res. Commun.*, **117**, 479–485.
Royer, C.A., Hinck, A.P., Loh, S.N., Prehoda, K.E., Peng, X., Jonas, J. and Markley, J.L. (1993) *Biochemistry*, **32**, 5222–5232.
Stites, W.E., Gittis, A.G., Lattman, E.E. and Shortle, D. (1991) *J. Mol. Biol.*, **221**, 7–14.
Tate, S., Ushioda, T., Utsunomiya-Tate, N., Shibuya, K., Ohyama, Y., Nakano, Y., Kaji, H., Inagaki, F., Samejima, T. and Kainosho, M. (1995) *Biochemistry*, **34**, 14637–14648.
Torchia, D.A., Sparks, S.W. and Bax, A. (1988) *Biochemistry*, **27**, 5135–5141.
Torchia, D.A., Sparks, S.W. and Bax, A. (1989) *Biochemistry*, **28**, 5509–5524.
Truckses, D.M., Somoza, J.R., Prehoda, K.E. and Markley, J.L. (1996) *Protein Sci.*, **5**, 1907–1916.
Wagner, G., Braun, W., Havel, T.F., Schaumann, T., Gō, N. and Wüthrich, K. (1987) *J. Mol. Biol.*, **196**, 611–641.
Wang, J., Hinck, A.P., Loh, S.N. and Markley, J.L. (1990a) *Biochemistry*, **29**, 102–113.
Wang, J., Hinck, A.P., Loh, S.N. and Markley, J.L. (1990b) *Biochemistry*, **29**, 4242–4253.
Wang, J., LeMaster, D.M. and Markley, J.L. (1990c) *Biochemistry*, **29**, 88–101.
Wang, J., Hinck, A.P., Loh, S.N., LeMaster, D.M. and Markley, J.L. (1992a) *Biochemistry*, **31**, 921–936.
Wang, J., Mooberry, E.S., Walkenhorst, W.F. and Markley, J.L. (1992b) *Biochemistry*, **31**, 911–920.
Wishart, D.S., Bigam, C.G., Yao, J., Abildgaard, F., Dyson, H.J., Oldfield, E., Markley, J.L. and Sykes, B.D. (1995) *J. Biomol. NMR*, **6**, 135–140.
Wüthrich, K., Billeter, M. and Braun, W. (1983) *J. Mol. Biol.*, **169**, 949–961.
Wüthrich, K. (1986) *NMR of Proteins and Nucleic Acids*, Wiley, New York, NY, U.S.A.
Zuiderweg, E.R.P., Boelens, R. and Kaptein, R. (1985) *Biopolymers*, **24**, 601–611.